Ore Geology Reviews 120 (2020) 103418

Contents lists available at ScienceDirect

Ore Geology Reviews

journal homepage: www.elsevier.com/locate/oregeorev

The relationship between the Taihe Fe-Ti oxide ore-bearing layered intrusion and the adjacent peralkaline A-type granitic pluton in SW China: Constraints from compositions of amphiboles and apatite-hosted melt inclusions

Kun Wang[a,b,c], Zhong-Yuan Ren[b,*], Le Zhang[b], Quan Ou[d]

[a] Key Laboratory of Mineralogy and Metallogeny, Guangzhou Institute of Geochemistry, Chinese Academy of Sciences, Guangzhou 510640, China
[b] State Key Laboratory of Isotope Geochemistry, Guangzhou Institute of Geochemistry, Chinese Academy of Sciences, Guangzhou 510640, China
[c] School of Earth Sciences, China University of Geosciences, Wuhan 430074, China
[d] School of Geosciences and Info-Physics, Central South University, Changsha 410083, China

ARTICLE INFO

Keywords:
Fe-Ti oxide ore
Layered intrusion
Melt inclusions
Amphibole
ELIP

ABSTRACT

The Taihe igneous complex, which is located in the inner zone of the Emeishan Large Igneous Province (ELIP), consists of an Fe-Ti oxide ore-bearing layered gabbroic unit and a silicic enclave-bearing peralkaline A-type granitic unit. The apatite-hosted melt inclusions in the gabbroic unit and the amphiboles in both the gabbroic unit and the granitic unit were used to investigate the relationship between the two units. The apatite-hosted melt inclusions have 32.3–68.3 wt% SiO_2, 0.51–23.9 wt% FeO_t, 0–7.19 wt% TiO_2, 8.87–19.0 wt% Al_2O_3, 2.39–19.5 wt% CaO, 1.70–7.27 wt% Na_2O, 0.24–5.60 wt% K_2O, and 0.13–6.83 wt% P_2O_5. Such a large compositional range is difficult to be achieved through fractional crystallization but can be accounted for by silicate liquid immiscibility developed during the differentiation of the gabbroic unit. The weighted bulk composition of the Taihe gabbroic unit is extremely rich in Fe and poor in Si (17.2 wt% FeO_t and 36.2 wt% SiO_2), indicating that some Si-rich components must have been removed. A significant compositional gap in the amphiboles in the gabbroic rocks and the adjacent peralkaline A-type granitoids, i.e., calcic amphibole in the gabbros and apatite-hosted inclusions and sodic-calcic to sodic amphiboles in the granites and their silicic enclaves, was observed. This cannot be explained by the previously suggested differentiation of a common basaltic parental magma from gabbros to silicic enclaves and granites, indicating a sudden change in the physical-chemical conditions of the related magmas. We propose that the silicic enclaves enclosed in the peralkaline A-type granitic pluton represent the missing Si-rich components of the Taihe layered gabbroic unit. The continuous expulsion of immiscible Si-rich melts from the lower crystal mush into the upper main magma body caused the crystallization of large amounts of Fe-Ti oxides in the gabbroic unit. Then, the residual Si-rich magmas in the upper part of the Taihe mafic magma chamber were drawn into the subsequently intruding peralkaline granitic magmas during the magmatic transgression process, forming the silicic enclaves within the adjacent contemporaneous peralkaline A-type granitic pluton.

1. Introduction

Mafic-ultramafic layered intrusions may host important mineral resources, such as Cu-Ni-PGE, Fe-Ti oxides, and chromite deposits. A close association is commonly observed between layered intrusions and granitic/rhyolitic rocks in various geological settings including intraplate, continental rift, and subduction zone (Bonin, 2007; Namur et al., 2010; Shellnutt and Zhou, 2007; Shellnutt et al., 2010; Shellnutt and Iizuka, 2011; VanTongeren and Mathez, 2012). One outstanding issue is the relationship between the mafic and felsic endmembers, which may have significant economic implications if they are genetically related to the formation of the ore deposits.

In the Emeishan Large Igneous Province (ELIP), SW China, layered intrusions hosting Fe-Ti oxide deposits are often spatially, temporally, and chemically associated with peralkaline A-type granitic plutons (Shellnutt and Zhou, 2007). It has been suggested that the peralkaline A-type granitic plutons were derived from partial melting of juvenile crust (Xu et al., 2008) or were cogenetic, but not comagmatic, with the

* Corresponding author.
E-mail address: zyren@gig.ac.cn (Z.-Y. Ren).

https://doi.org/10.1016/j.oregeorev.2020.103418
Received 5 November 2019; Received in revised form 12 February 2020; Accepted 17 February 2020
Available online 19 February 2020
0169-1368/

mafic–ultramafic intrusions (Zhong et al., 2007, 2011). Nevertheless, the close proximity between the two units has also led to the speculation that the peralkaline A-type granitic plutons represent the differentiation products of the Fe-Ti oxide ore-bearing layered intrusions through fractional crystallization (Shellnutt and Zhou, 2007; Shellnutt et al., 2009, 2010, 2011) or silicate liquid immiscibility (Liu et al., 2016). The comagmatic formation from a common parental magma is a reasonable explanation for the geochemical and geochronological data and can account for the enrichment of Fe-Ti oxides in the layered intrusions (Shellnutt et al., 2009). According to studies of Thingmuli and other Iceland volcanoes, only 5%–10% total felsic melts can be differentiated from a basaltic magma (Carmichael, 1964). The silicic rocks produced by the Skaergaard, Bushveld, and Sept Iles original magmas account for ~8%, ~9%, and ~8% of their entire igneous bodies, respectively (Veksler, 2009; VanTongeren et al., 2010; Namur et al., 2011). However, in the ELIP, the peralkaline A-type granitic plutons are usually volumetrically larger than the associated oxide ore-bearing layered intrusions. In view of the mass ratios of these units, whether the concomitant mafic-granitic complexes are produced by a common parental magma must be considered. If not, we must consider whether any silicic rocks were differentiated from these layered intrusions. We must also investigate the nature of the possible corresponding geological products.

The well-exposed Taihe igneous complex in the northern part of the Panxi region consists of an oxide ore-bearing gabbroic unit and a peralkaline A-type granitic unit. It is an ideal situation for examining the genetic relationship between the spatially and temporally associated mafic and felsic rocks of the ELIP. In this study, apatite-hosted melt inclusions from the gabbroic unit and amphiboles from the different rocks of the two units are used to investigate the evolution process of the Taihe magma chamber and to investigate the relationship between the concomitant gabbroic-granitic complex.

2. Geologic background

The Late Permian (ca. 260 Ma) ELIP is exposed in the southwestern part of China and the northern part of Vietnam with an area of over 5×10^5 km^2 (Chung and Jahn, 1995; Xu et al., 2001). It mainly consists of flood basalt, mafic-ultramafic intrusions, felsic plutons, and a small amount of picrite, trachyte, and rhyolite. The Panxi region, in the inner zone of the ELIP, is marked by mafic–ultramafic layered intrusions hosting giant Fe-Ti oxide deposits, e.g., the Panzhihua, Hongge, Baima, Xinjie, and Taihe intrusions, which contain 1333 Mt, 4572 Mt, 1497 Mt, 410 Mt, and 810 Mt of ore reserves, respectively (Fig. 1a; Ma et al., 2003). These intrusions, together with the spatially and temporally associated continental flood basalts and the granitic-syenitic plutons, were summarized as the trinity, which was treated as the sign for the regional prospecting of Fe-Ti oxide deposits (Zhang et al., 1988).

Based on the lithologic variations, the Fe-Ti oxide ore-bearing layered intrusions in the Panxi region can be roughly divided into two categories. The first consists of the entire mafic–ultramafic layered sequence of ultramafic rocks (peridotite and/or pyroxenite) in the lower part and gabbroic rocks in the upper part, such as the Hongge and Xinjie intrusions. The second is mainly composed of gabbros and/or troctolites with few ultramafic rocks, such as the Panzhihua, Baima, and Taihe intrusions. Despite this, all of these intrusions share a common feature, i.e., major ore bodies occur in the lower horizons of the intrusions, and the ore bodies are volumetrically large compared to layered intrusions elsewhere in the world. For example, magnetite ores occur in the upper zone of the Bushveld Complex (~6500 m thick), and the total thickness of the ore layers with > 50% magnetite is only 20.4 m (Tegner et al., 2006). However, the about 2000-m-thick Panzhihua intrusion hosts a 60-m-thick massive ore body in its basal part, and the banded ores in the upper part are 80–400 m thick with an average thickness of 100 m (Qiu and Xie, 1988). The oxide-rich and oxide-poor layers commonly alternate throughout the sequence of the layered intrusions in the Panxi region. The unique Fe-Ti oxide deposits in the Panxi region were termed Panzhihua type (Zhou et al., 2013).

The Taihe gabbroic layered intrusion is located 12 km west of Xichang City in Sichuan Province. It is ~1.4 km thick, extends ~3 km NE-SW, dipping 50°–60° SE, and has an outcrop area of ~13 km^2 (Fig. 1b) (Hou et al., 2012; She et al., 2014, 2015). U-Pb zircon dating indicates that the intrusion formed at 259 ± 3 Ma (She et al., 2014). The intrusion has been extensively exposed by mining activity (Fig. 2a). It exhibits good igneous rhythmic layering (Fig. 2b) with three-group joints in the NE-SW, NW-SE, and N-S directions, which dislocate the layering locally. The layering is cut through by several granitic dikes, which are 0.5–10 m wide and tens to hundreds of meters long. To the west of the Taihe layered intrusion is the peralkaline A-type granite, which is well exposed by a chain of quarries in the surrounding highland (Fig. 2c and d). The Taihe peralkaline A-type granite is 261 ± 2 Ma (Xu et al., 2008). It is considered to be fault-bound by the gabbroic intrusions and the high-Ti flood basalts (Zhang et al., 1988).

3. Petrography

3.1. Lithology of the gabbroic layered unit and the peralkaline granitic unit

The Taihe gabbroic layered unit is divided into three zones including the lower zone (LZ), the middle zone (MZ), and the upper zone (UZ), based on rock texture, mineral assemblage, and ore mineral abundances (Li et al., 1981). The LZ mainly consists of olivine-bearing gabbro with olivine clinopyroxenite interlayers. The olivine-bearing gabbro contains 30–50 vol% clinopyroxene, 30–60 vol% plagioclase, 5–15 vol% Fe-Ti oxides, and < 10 vol% olivine. The olivine clinopyroxenite is composed of 50–70 vol% clinopyroxene, 20–30 vol% olivine, 5–15 vol% plagioclase, and 5–10 vol% Fe-Ti oxides. The MZ is the main ore-bearing zone, which consists of Fe-Ti oxide ores, gabbro, and oxide-rich clinopyroxenite (Fig. 3a and b). The major gangue minerals in the ores are clinopyroxene and plagioclase with minor amounts of olivine (Fig. 4a). The higher the Fe-Ti oxide contents of the ores, the greater the proportion of clinopyroxene in the gangue minerals. The gabbro is composed of 30–50 vol% plagioclase, 30–50 vol% clinopyroxene, 5–30 vol% Fe-Ti oxides, < 8 vol% apatite, and < 5 vol% amphibole (Fig. 4b). The oxide-rich clinopyroxenite contains 40–70 vol% clinopyroxene, 10–30 vol% Fe-Ti oxides, < 15 vol% plagioclase, < 10 vol % apatite, and < 5 vol% amphibole. The UZ is mainly composed of apatite gabbro with clinopyroxenite interlayers. Compared with the gabbro in the MZ, the apatite gabbro in the UZ has more plagioclase and apatite, but less clinopyroxene and Fe-Ti oxides. It is composed of 40–70 vol% plagioclase, 10–40 vol% clinopyroxene, 5–15 vol% Fe-Ti oxides, 3–10 vol% apatite, and 3–10 vol% amphibole (Fig. 4c). The mineral assemblage of the clinopyroxenite in the UZ is similar to that of the congener rock in the MZ but has a much lower Fe-Ti oxides content.

For the entire sequence of the Taihe layered unit, clinopyroxene and plagioclase are the major cumulate phases, and they are partially or completely enclosed by interconnected Fe-Ti oxides. It should be noted that the clinopyroxene grains are often Fe-Ti-rich and contain oxide exsolution lamellae parallel to the prismatic cleavage planes (Fig. 4d). The plagioclase generally occurs as anhedral to subhedral platy grains. Most of the apatite grains are closely associated with the Fe-Ti oxides and occupy the interstitial spaces between the silicate minerals (Fig. 4b–d). A small amount of apatite is enclosed within the clinopyroxene and plagioclase grains (Fig. 4d).

The peralkaline A-type granites adjacent to the Taihe layered unit are coarse-grained and are composed of 65% alkali feldspar, 25% quartz, < 10% amphibole, and a minor amount of accessory minerals, such as titanite, zircon, fluorite, and biotite (Fig. 4e). They contain centimeter-sized melanocratic enclaves (Fig. 3c and d). Most of the enclaves are ellipsoidal (Fig. 3c), but a few are irregular in shape (Fig. 3d). The enclaves are fine-grained, which distinguishes them from the host granite, and they consist primarily of 60%–70% alkali feldspar,

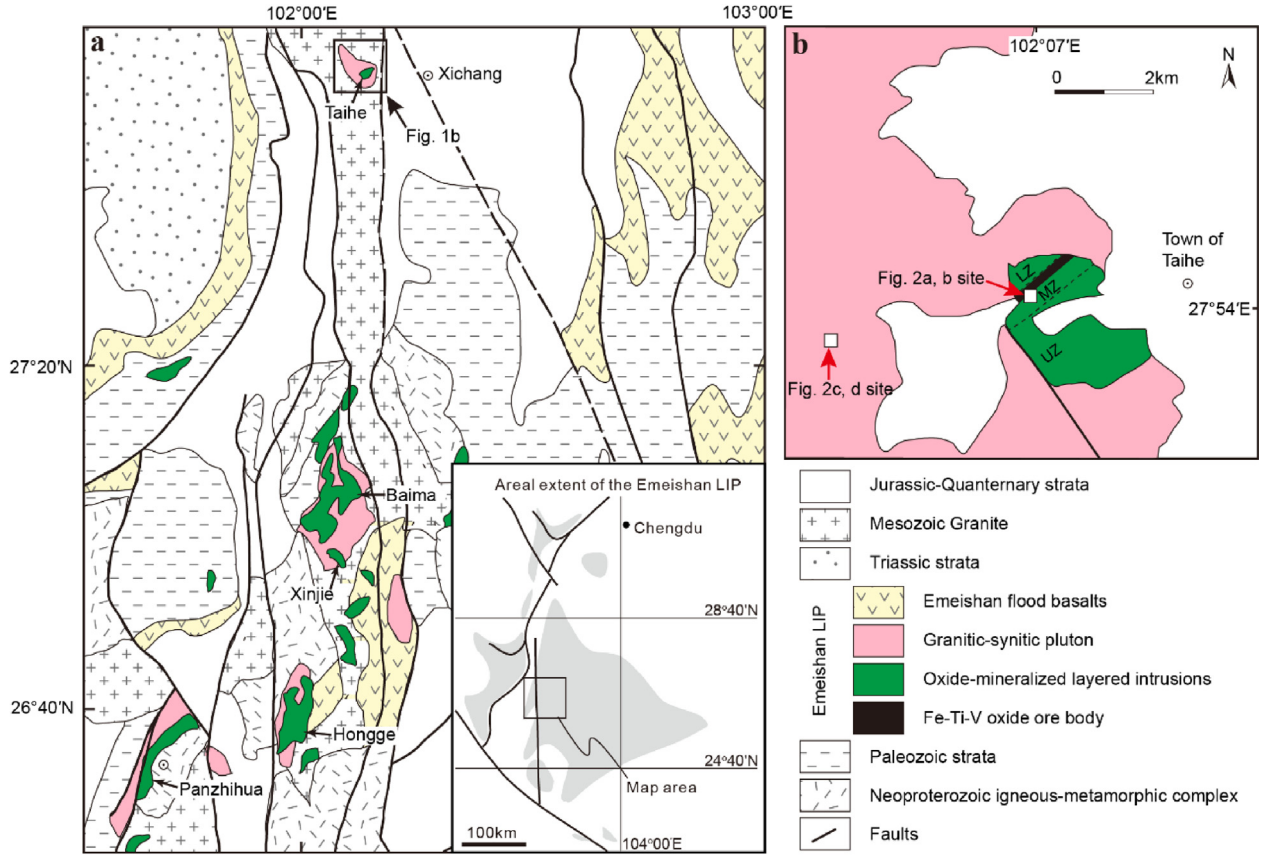

Fig. 1. (a) Geological map of the Panxi region showing the distribution of mafic–ultramafic layered intrusions, granitic-syenitic plutons and the Emeishan flood basalts (modified after Pang et al., 2009). (b) Simplified geological map of the Taihe gabbroic-granitic complex.

5%–20% quartz, and 10%–25% amphibole (Fig. 4f). Most of the alkali feldspar crystals are euhedral to subhedral and are 100–500 μm in length with perthitic exsolution lamellae. Rare extremely coarse-grained alkali feldspars similar in size to those in the host granite were observed in the enclaves.

3.2. Apatite-hosted melt inclusions from the gabbroic unit

Apatite is a common phase in various types of cumulate rocks throughout the MZ and UZ of the Taihe intrusion. The apatite crystals in these rocks share common characteristics. They are subhedral to euhedral in shape and are 100–500 μm long. Some of the crystals contain one or more inclusions, while others do not contain inclusions. The melt inclusions in the apatite are light to dark brown and are rounded, oval, polygonal, or elongated in shape (Fig. 5a–d). They range from 5 to 50 μm in width and from 10 to 100 μm in length. All of the inclusions are holocrystalline, multiphase, mineral aggregates with irregular outlines. Most of the inclusions are composed of several of the daughter phases, including amphibole, plagioclase/albite, clinopyroxene, and minor amounts of magnetite, ilmenite, and K-feldspar (Fig. 5e and f). A small number of the inclusions also contain biotite and sulfides. Although the proportion of the daughter phases is highly variable, amphibole is often a dominant phase in many of the inclusions, but it is absent in some of the inclusions.

3.3. Amphibole from the gabbroic unit and the peralkaline granitic unit

Brown amphiboles were generally observed in the gabbroic rocks. They occur as rims on the plagioclase and clinopyroxene, especially when the plagioclase and clinopyroxene are in contact with the Fe-Ti oxides (Fig. 4c). The amphibole in the peralkaline A-type granite is subhedral and interstitial to the alkali feldspar and quartz, accounting for < 10% of the mineral mode (Fig. 4e). The pleochroism is conspicuous, varying from green to blue to puce. In the enclaves, the amphibole is subhedral to anhedral and is interstitial to the alkali feldspar, comprising 10%–25% of the mineral mode (Fig. 4f). Most of the amphibole grains are greenish-blue, but some are reddish-brown. The grains are much smaller than those in the peralkaline A-type granite hosting the enclaves.

4. Sampling and analytical methods

The samples used in this study were collected from an open-pit mine in the Taihe layered intrusion and a quarry in the adjacent granite pluton. Apatite grains from eight apatite-bearing gabbroic rocks were separated to study the apatite-hosted melt inclusions. The compositions of the amphibole in five gabbros, four peralkaline granites, and four silicic enclaves were analyzed.

4.1. Homogenization of the apatite-hosted melt inclusions

Homogenization of crystallized melt inclusions hosted in apatite was performed in the Melt Inclusion Laboratory at the Guangzhou Institute of Geochemistry (GIG), Chinese Academy of Sciences (CAS). The same heating conditions were used as those for homogenization of crystallized melt inclusions in the apatite of the Sept Iles intrusion (Charlier et al., 2011). The heating procedures followed those described by Ren et al. (2017). The apatite grains were placed in a small platinum bag, and then, they were gradually heated from 100 °C to 1100 °C within two hours, after which, they were kept at 1100 °C for 30 min. The pressure was maintained at 1 atm and the oxygen fugacity controlled at QFM-1 using a CO_2-H_2 gas mixture during the heating

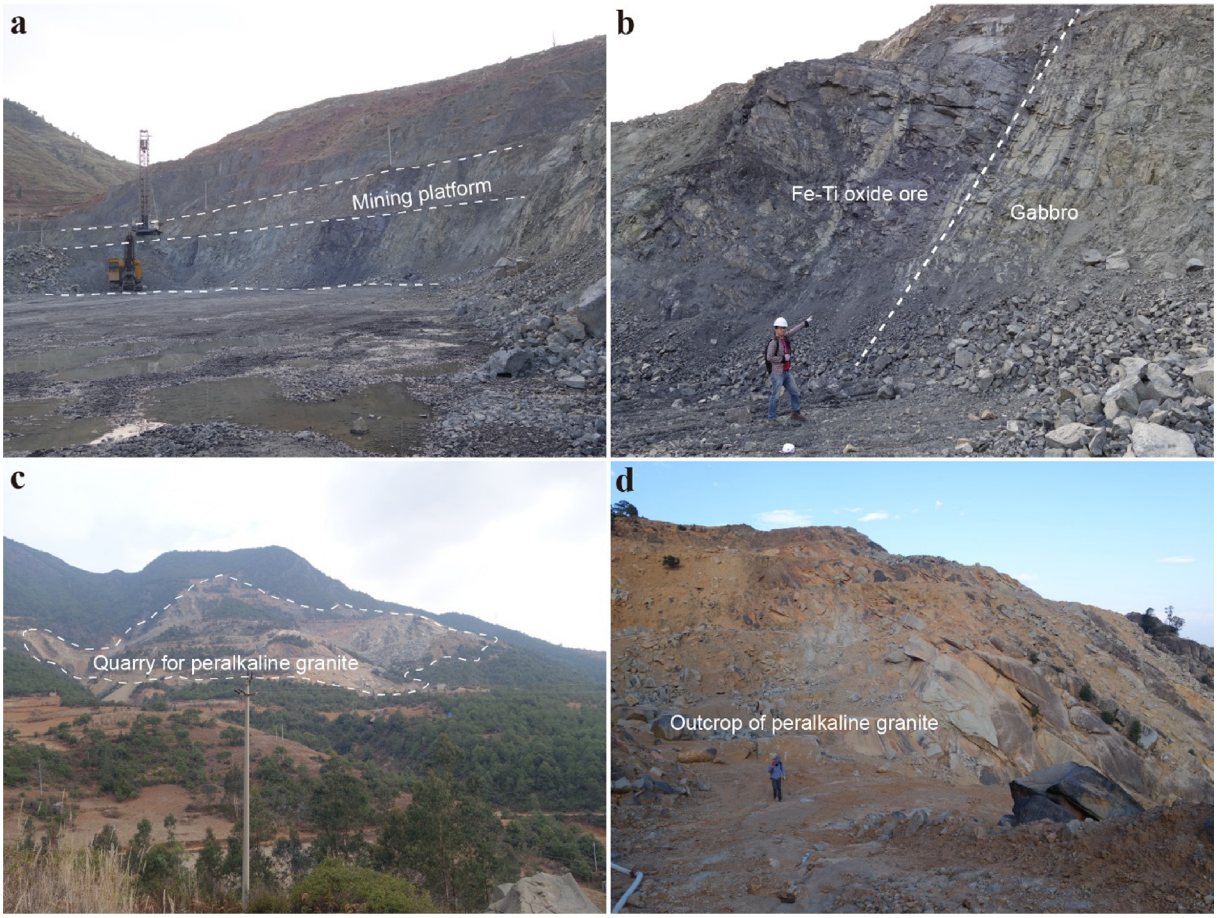

Fig. 2. Field photographs of Taihe gabbroic-granitic complex. (a) An open-pit mining work platforms within the Taihe gabbroic intrusion; (b) Layered Fe-Ti oxide ore body and gabbroic rocks; (c) A quarry for peralkaline A-type granite within the exposed Taihe granitic pluton; (d) An outcrop of the peralkaline A-type granite.

process. Then, the reheated grains were rapidly removed from the furnace and quenched in the air. The quenched grains were mounted in epoxy resin and polished to expose the melt inclusions for electron microprobe analysis.

4.2. Compositional analysis of the melt inclusions and minerals

The compositions of the apatite-hosted melt inclusions and the amphiboles were analyzed using a JEOL JXA 8230 electron microprobe at the Key Laboratory of Mineralogy and Metallogeny, GIG-CAS.

The operating conditions used for the melt inclusion analyses were as follows: accelerating voltage of 15 kV, beam current of 10nA, and defocused beam of 3 μm. The Na and K were analyzed first to minimize their loss during the analyses. The peak and background counting times were 10 s and 5 s, respectively, for Na and K; 20 s and 10 s for Fe, Mg, Ca, Al, and Si; and 40 s and 20 s for P, Ti, and Mn. The standards used were chrome-diopside for Ca and Si, almandine for Fe and Al, periclase for Mg, rutile for Ti, rhodonite for Mn, albite for Na, orthoclase for K, and apatite for P. The raw data were reduced using the ZAF correction method.

The operating conditions used for the amphibole analyses were as follows: accelerating voltage of 15 kV, beam current of 20nA, and beam diameter of 1 μm. Na and K were analyzed first to reduce the migration effect. The peak and background counting times were 10 s and 5 s, respectively, for Na and K; 20 s and 10 s for Fe, Mg, Ca, Al, and Si; and 40 s and 20 s for P, Ti, and Mn. The following standards were used: kaersutite for Si, Al, Ca, and Fe; periclase for Mg, rutile for Ti, rhodonite for Mn, albite for Na, orthoclase for K, and apatite for P. The analytical results were reduced using the ZAF correction method.

5. Results

5.1. Characteristics of the apatite-hosted melt inclusions after homogenization

After heating and quenching, some inclusions contained single homogeneous melt phases with gas bubbles (Fig. 6a and b), while others still contained a few unmelted phases, e.g., magnetite, plagioclase, and clinopyroxene (Fig. 6c and d). The unhomogenized inclusions containing unmelted phases may be the result of complex processes related to their formation or to post-entrapment modification. For example, the presence of some unmelted magnetite is largely due to the reaction $3FeO + H_2O \rightarrow Fe_3O_4 + H_2$ after entrapment, during which the irreversible loss of H_2 occurs (Danyushevsky et al. 2002). Additionally, residual phases such as plagioclase and clinopyroxene may indicate the heterogeneous trapping of crystals within the melt pocket during the formation of the inclusion (Kent, 2008; Jakobsen et al., 2011). Thus, it is difficult to completely homogenize these inclusions by heating them.

5.2. Compositions of the quenched apatite-hosted melt inclusions

The glass compositions of the quenched apatite-hosted melt inclusions are reported in Table 1. The homogenized melt inclusions contain 51.4–68.3 wt% SiO_2 and 0.51–5.91 wt% FeO_t. The glass in the unhomogenized inclusions contain 32.3–58.9 wt% SiO_2 and 2.49–23.9 wt % FeO_t, i.e., they are relatively richer in Fe and poorer in Si than the homogenized inclusions. Because of possible chemical modification, caution must be exercised when interpreting the unhomogenized

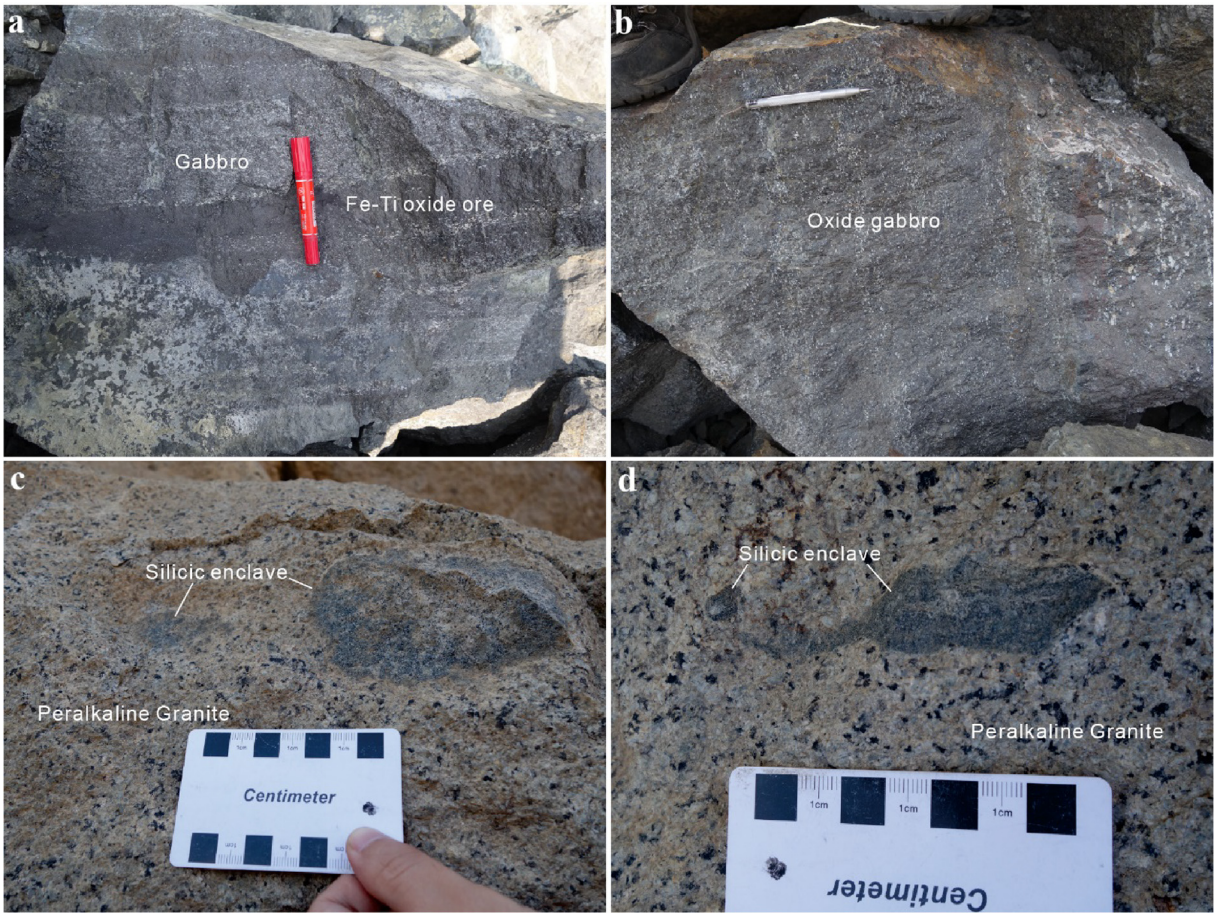

Fig. 3. Photographs showing the occurrence of the different rocks in the Taihe gabbroic-granitic complex. (a) Centimeter-scale bands of Fe-Ti oxide ores and gabbros; (b) Rhythmic layering of plagioclases in the oxide-rich gabbro; (c) Elliptoid silicic enclaves in the peralkaline A-type granite; (d) Irregular shaped silicic enclaves in the peralkaline A-type granite.

inclusions. In fact, some of the unhomogenized inclusions may have higher FeO_t contents than the measured values due to the irreversible crystallization of magnetite. However, the extent of crystallization is expected to be small because magnetite is not a common residual phase. Another factor that needs to be considered is the heating temperature since overheating can introduce the compositions of trapped solids and host apatite into the melts. The low P_2O_5 contents (low to 0.13 wt%) of those homogenized inclusions suggest that there was no excessive melting of the host apatite, and 1100 °C is not an overheating temperature. Thus, the trapped primocrysts had little effect on the glass compositions of the unhomogenized inclusions because they would only have melted at abnormally high temperatures. Overall, the melt inclusions have highly variable major element compositions with SiO_2 contents ranging from 32.3 to 68.3 wt%, FeO_t from 0.51 to 23.9 wt%, TiO_2 from 0 to 7.19 wt%, Al_2O_3 from 8.87 to 19.0 wt%, CaO from 2.39 to 19.5 wt%, Na_2O from 1.70 to 7.27 wt%, K_2O from 0.24 to 5.60 wt%, and P_2O_5 from 0.13 to 6.83 wt%. On the plots of SiO_2 versus $FeO_t + TiO_2 + P_2O_5$ and SiO_2 versus $Al_2O_3 + Na_2O + K_2O$, the inclusions form continuous trends comparable to the apatite-hosted melt inclusions from the Panzhihua, Sept Iles, and Bushveld intrusion (Charlier et al., 2011; Fischer et al., 2016; Wang et al., 2018) (Fig. 7a and b).

5.3. Compositions of the amphibole from the different rock types

Representative analyses of amphibole grains from the gabbroic rocks, apatite-hosted inclusions, granite, and silicic enclaves are reported in Supplementary Table S1. Calculations, including ferric-ferrous estimates, were made on a 23(O) basis, following the method of Leake et al. (2004) and Esawi (2004). The amphibole in the apatite-hosted inclusions contained 1.21–3.13 wt% Na_2O, 9.98–13.2 wt% CaO, 35.6–47.6 wt% SiO_2, and Mg# of 34–76, which are similar to those of the amphibole from the gabbroic rocks (1.50–3.58 wt% Na_2O, 10.7–12.3 wt% CaO, 35.9–43.8 wt% SiO_2, and Mg# of 20–72). All of the amphibole grains analyzed are calcic-amphiboles, such as pargasite, ferropargasite, magnesiohastingsite, and hastingsite. However, the amphibole in the enclaves and granites have compositions of 5.65–11.9 wt% Na_2O, 0.22–8.50 wt% CaO, and 49.3–51.6 wt% SiO_2 and 4.60–12.5 wt% Na_2O, 0–9.98 wt% CaO, and 48.5–52.2 wt% SiO_2, respectively. Both span from sodic-calcic to sodic compositions, but the dominant compositions are sodic-calcic amphiboles, e.g., ferro-richterite, in the silicic enclaves, and sodic amphiboles, e.g., ferroeckermannite and riebeckite, in the peralkaline A-type granite.

6. Discussion

6.1. Liquid immiscibility revealed by the apatite-hosted melt inclusions

The daughter amphibole in the crystallized inclusions within the apatite of the Taihe layered intrusion has Mg# ranging from 76 to 34, which indicates that these apatite grains did not form at the same time but crystallized from melts at different differentiation stages over a temperature interval. The large compositional variation (32.3–68.3 wt % SiO_2) of the apatite-hosted melt inclusions may be caused either by fractional crystallization or by liquid immiscibility (cf. Fischer et al., 2016). In order to test the first hypothesis, the liquid line of descent

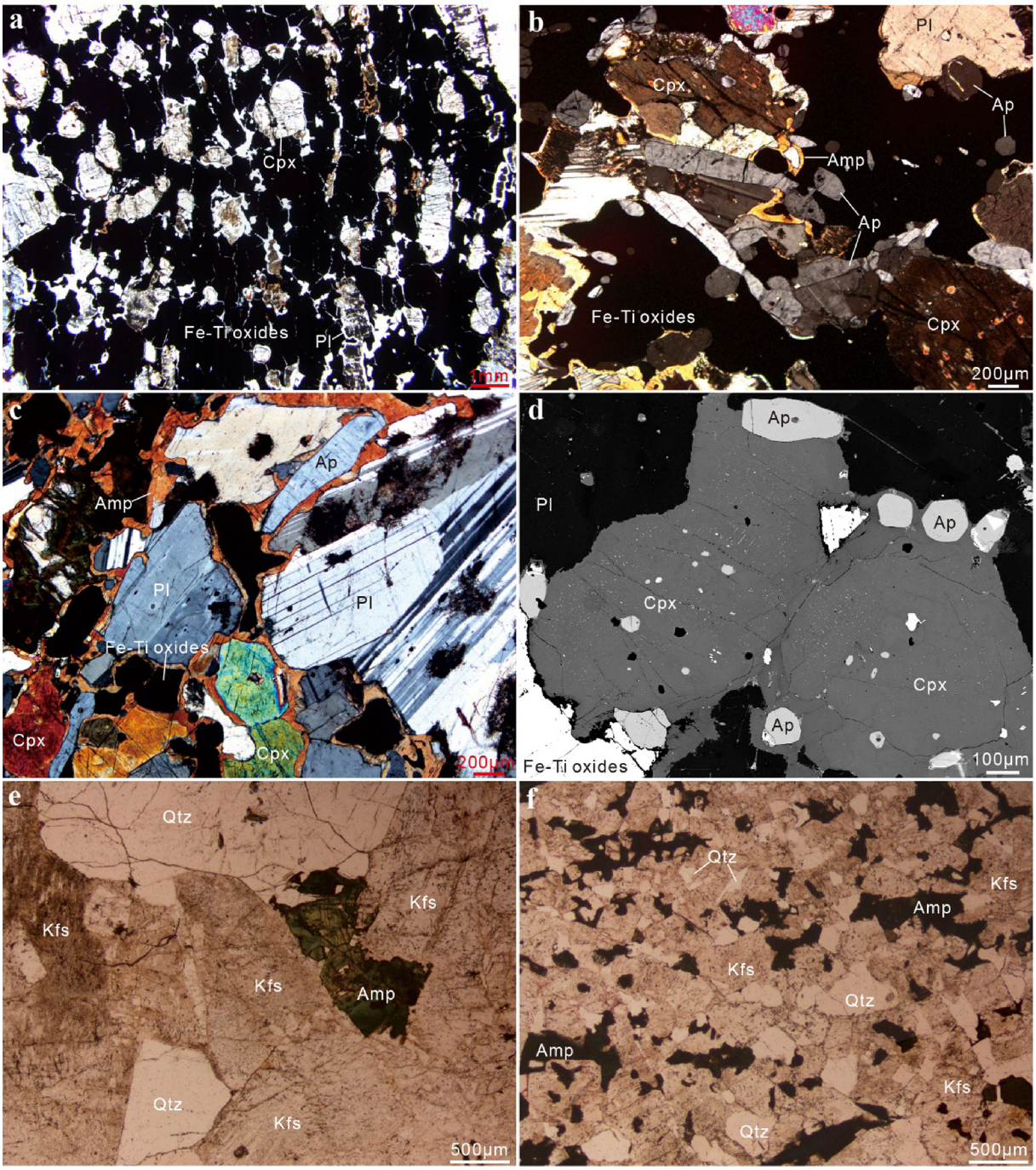

Fig. 4. Microphotographs of the major lithologies of the Taihe gabbroic-granitic complex. (a) Net-textured ores showing that silicate minerals are surrounded by a network of Fe-Ti oxides, under plane-polarized light; (b) Apatite-bearing oxide gabbro composed of cumulus plagioclase (Pl), clinopyroxene (Cpx) and apatite (Ap) with interstitial Fe-Ti oxides, under cross-polarized light; (c) Apatite gabbro showing widely developed amphibole (Amp) rims between primocrysts and interstitial Fe-Ti oxides, under cross-polarized light; (d) Clinopyroxene has exsolution lamellaes of Fe-Ti oxides which are shown by weeny white dots within the clinopyroxene grains, BSE image; (e) Coarse-grained peralkaline A-type granite composed of Quartz (Qtz), alkaline feldspar (Kfs) and amphibole (Amp), under plane-polarized light; (f) Fine-grained silicic enclave composed of Quartz, alkaline feldspar and amphibole, under plane-polarized light.

(LLD) for the Taihe intrusion was simulated using the MELTS thermodynamic algorithm (Ghiorso and Sack, 1995). Since the Fe-Ti oxide ore-bearing layered intrusions in the Panxi region are believed to be derived from the high-Ti basalt or picrite in the ELIP (Hou et al., 2012; Zhou et al., 2013), we choose four lavas with high-Ti affinities (Lijiang picrite DJ-2 from Zhang et al., 2006; Ertan basalt EM-78 from Xu et al., 2001; Binchuan basalt WL17-20 from Xiao et al., 2004; Songda basalt HK-43 from Wang et al., 2007) as the starting compositions to model their potential differentiation trends under various conditions with initial H_2O contents of 0.1 and 1.0 wt%; oxygen fugacities (fO_2) of QFM-1, QFM, and QFM + 1; and pressures of 2 kbar and 5 kbar. The results for the starting compositions of EM-78 and DJ-2 record a stage of FeO_t-enrichment and SiO_2-depletion before magnetite saturation (Fig. 8a). After magnetite saturation, the residual melts turn towards SiO_2-enrichment. An extreme Fe-rich melt with 24.5 wt% FeO_t and 47.5 wt% SiO_2 was produced when picritic magma DJ-2 with 0.1 wt% H_2O differentiated through fractional crystallization at a pressure of 5 kbar and fO_2 of QFM-1. The results for the other starting compositions show a

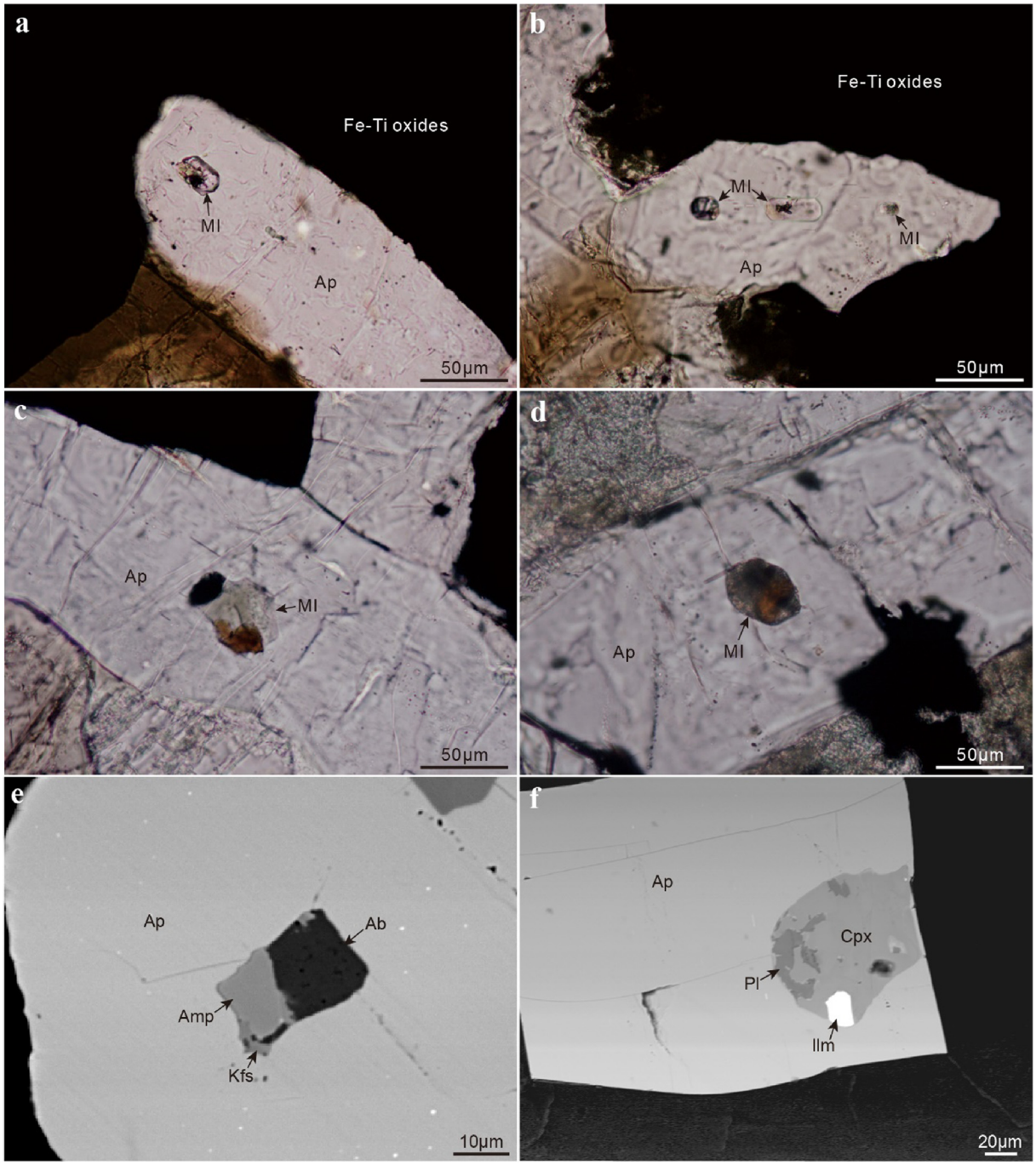

Fig. 5. Microphotographs of the crystallized melt inclusions (MI) within apatite (Ap) from the Taihe gabbroic intrusion. (a) An oval-like light-colored inclusion, under plane-polarized light; (b) Dark- and light- colored inclusions within a single apatite, under plane-polarized light; (c) A polygonal-shape inclusion composed of dark-, light-, and brown- colored phases, under plane-polarized light; (d) An oval-like brown-colored inclusion, under plane-polarized light; (e) An inclusion containing amphibole (Amp), albite (Ab), and K-feldspar (Kfs), BSE image; (f) An inclusion containing clinopyroxene (Cpx), plagioclase (Pl), and ilmenite (Ilm), BSE image.

consistent trend of FeO_t-depletion and SiO_2-enrichment (Fig. 8a). Whatever the starting composition, oxygen fugacity, and initial H_2O contents, Si-poor and Fe-rich melts with < 40 wt% SiO_2 and > 10 wt% FeO_t for the Taihe melt inclusions never occur as a potential fractional crystallization trend. The only explanation that we can offer for these Si-poor and Fe-rich melt inclusions is the involvement of liquid immiscibility during the evolution of the Taihe layered intrusion. If this is the case, the Si-rich melt inclusions could also have been produced by liquid immiscibility and could represent the conjugate immiscible Si-rich melts of the Fe-rich melt inclusions.

On the pseudo-ternary Greig diagram (Fig. 8b), the apatite-hosted melt inclusions plot close to the two-liquid field of the leucite-fayalite-silica system (Roedder, 1951), and their distribution trends are perfectly parallel to the tie line of the conjugated immiscible melts of the experimental products (Mcbirney and Nakamura, 1974; Dixon and Rutherford, 1979; Longhi, 1990; Veksler et al., 2007) and the natural samples (Philpotts, 1982; Ryabov, 1989; Charlier et al., 2011; Wang et al., 2018). It has been suggested that the two-liquid field of the natural magma, especially a system with high Fe, Ti, and P contents, expands toward more alkali- and alumina-rich compositions (Freestone,

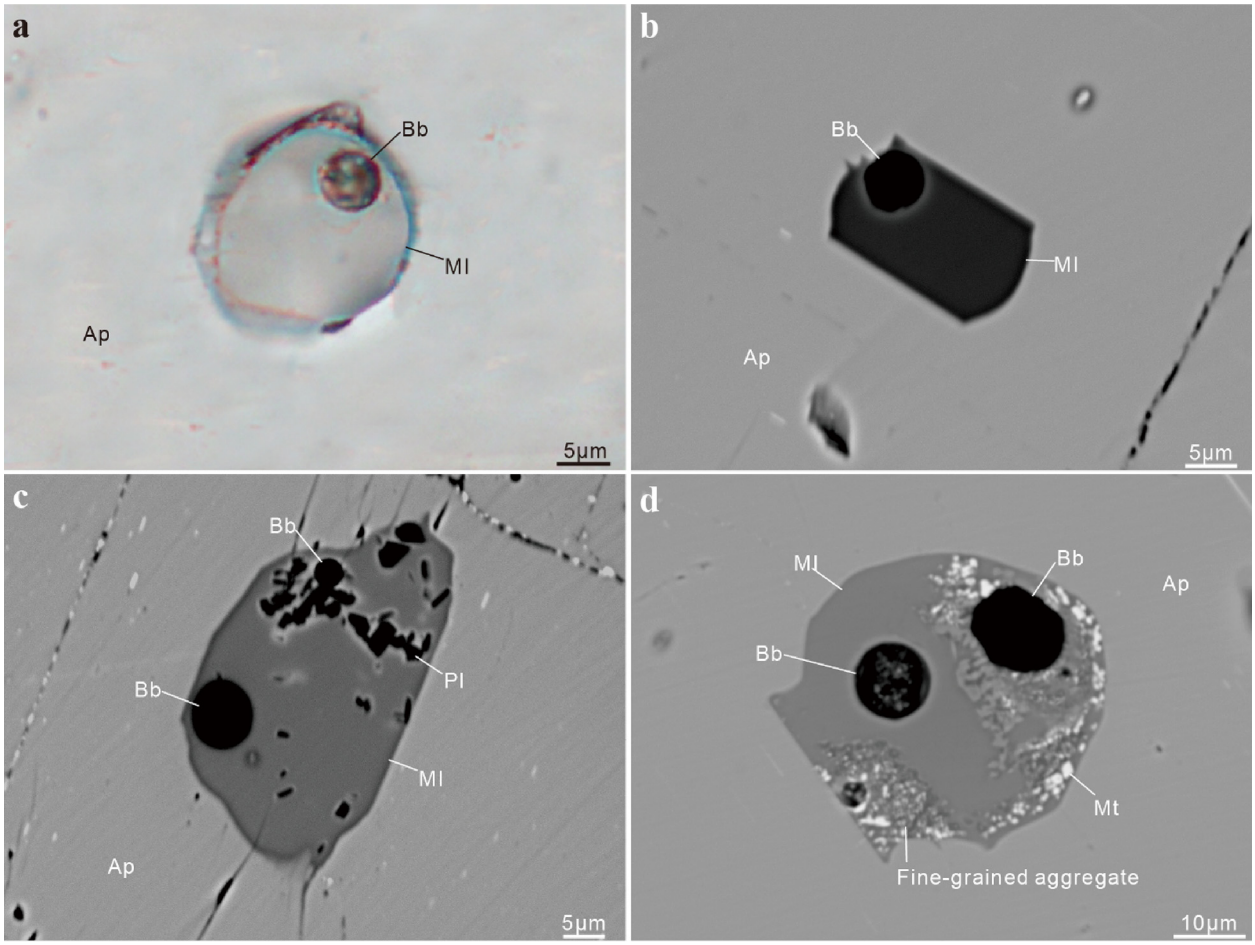

Fig. 6. Microphotographs and back-scattered electron (BSE) images of the reheated melt inclusions (MI) within apatite (Ap) from the Taihe gabbroic intrusion. (a) A rounded homogenized melt inclusion with a bubble (Bb), under transmitted polarized light; (b) An oval-like homogenized melt inclusion with a bubble, BSE image; (c) An unhomogenized melt inclusion containing glass, bubbles, and plagioclase (Pl) crystals, BSE image; (d) An unhomogenized melt inclusion containing glass, bubbles, magnetites (Mt), and unidentified fine-grained phases, BSE image.

1978; Visser and Van Groos, 1979; Eby, 1980; Naslund, 1983; Rajesh, 2003). This reconciles with the distribution of the melt inclusions analyzed in this study and those from the Panzhihua and Sept Iles intrusions (Charlier et al., 2011; Wang et al., 2018).

6.2. Extremely Fe-rich and Si-poor bulk composition of the Taihe layered intrusion

It is generally accepted that the Taihe layered intrusion is Fe-Ti-rich and Si-poor (Hou et al., 2012; She et al., 2014, 2015; Bai et al., 2016). The weighted average bulk composition of the intrusion, excluding the Fe-Ti oxide ore bodies, is 14.1 wt% FeO_t, 4.10 wt% TiO_2, and 43.1 wt% SiO_2 (Hou et al., 2012), which is extremely Fe- and Ti-rich and Si-poor compared to normal tholeiitic magmas (Table 2). Since the oxide ore bodies are important parts of the intrusion, if they are included in the bulk composition, the entire intrusion would be even richer in Fe and Ti and more depleted in Si. We calculated the bulk composition of the entire intrusion including the ore bodies based on the composition and thickness of each component of the intrusion and on the entire lithologic column (data from Hou et al., 2012; She et al., 2014), which yields a composition containing 17.2 wt% FeO_t, 4.78 wt% TiO_2, and 36.2 wt% SiO_2 (Table 2).

It is puzzling how such an Fe-Ti-rich and Si-poor magma was generated. Although ferrobasalts are usually Fe-Ti-rich, Fe and Ti enrichment combined with SiO_2 depletion is rare in terrestrial basalts and their deuterogenic magmas (Yoder and Tilley, 1962; Kushiro, 1979). Several studies have suggested that the Fe-Ti-rich and Si-poor parental magma of the Taihe layered intrusion was produced by the interaction between the Emeishan plume and the lithospheric mantle, which contained an eclogite component (Hou et al., 2011, 2012). However, it is still debated whether partial melting of the eclogite component could produce a magma with the bulk composition of the Taihe layered intrusion since it is much richer in Fe and poorer in Si than the Emeishan picrite (Table 2). Such an extremely Fe-rich melt would have a density of 2.96 g/cm^3, calculated based on the method of Bottinga and Weill (1970) at 1300 °C, which is much higher than the average density of continental crust (2.75 g/cm^3; Armstrong, 1991), so it does not easily migrate into the shallow crust. Thus, we suggest that the parental magma of the Taihe layered intrusion may be rich in Fe and Ti and poor in Si, but not to the degree suggested by the bulk composition of the solidified gabbroic unit. The current Taihe layered intrusion is only the residual Fe-rich part of the original magma, and a considerable quantity of Si-rich components has been removed from the Taihe magma chamber.

6.3. A possible link between the missing Si-rich component of the Taihe layered intrusion and the silicic enclaves in the adjacent peralkaline A-type granitic pluton

Finding the missing Si-rich component is an important issue, which bears on how the layered intrusion evolved and how the Fe-Ti oxides were concentrated. It was previously proposed that the Taihe layered

Table 1
Glass compositions (wt.%) of reheated melt inclusions in apatite from the Taihe gabbroic layered intrusion.

Sample	TH1566					TH1567					TH1569							
MI No.	1	2	3	4	5	1	2	3	4	5	1	2	3	4	5	6	7	8
State	UH	H	UH	UH	UH	H	H	H	UH	UH	H	UH	H	UH	H	H	H	H
SiO_2	40.5	68.0	37.6	33.4	38.8	62.3	64.7	68.0	58.9	55.4	61.0	36.6	51.3	57.0	60.3	59.7	52.6	58.8
TiO_2	0.41	0.05	1.41	0.20	0.81	0.04	0.13	0.00	1.32	3.34	0.15	3.52	0.27	1.19	0.11	0.28	0.00	0.05
Al_2O_3	15.2	17.8	14.9	8.87	12.1	16.3	16.8	17.0	18.7	15.1	17.8	12.3	15.7	16.5	17.7	17.2	15.3	16.5
FeO_t	12.2	0.85	12.8	23.9	14.4	2.53	1.69	0.51	2.49	6.42	2.67	10.9	5.00	4.50	2.25	2.23	4.09	4.67
MnO	0.21	0.01	0.18	0.21	0.19	0.05	0.10	0.03	0.09	0.09	0.04	0.26	0.07	0.10	0.04	0.13	0.06	0.06
MgO	5.04	0.36	5.13	3.31	5.70	1.19	0.62	0.13	1.74	2.01	0.67	6.53	4.27	2.20	1.58	1.49	2.09	1.16
CaO	14.4	2.84	16.3	19.5	14.5	6.61	4.38	2.39	6.37	6.84	7.98	14.6	10.2	6.54	7.07	6.91	11.6	7.19
Na_2O	3.19	6.76	3.62	1.70	4.29	4.01	5.97	5.78	5.60	4.50	4.63	3.79	4.16	4.29	4.10	7.08	3.70	4.98
K_2O	3.95	3.42	1.67	0.61	1.56	3.72	3.19	5.60	2.54	2.89	3.31	1.92	3.82	4.00	4.42	3.23	4.37	4.24
P_2O_5	4.12	0.28	4.55	5.32	4.99	0.98	0.93	0.13	1.44	2.19	0.88	6.83	3.34	1.64	1.33	1.28	4.04	1.59
Total	99.2	100	98.1	97.0	97.3	97.7	98.5	99.5	99.2	98.8	99.2	97.2	98.4	98.0	98.9	99.4	97.8	99.3

Sample	TH1570						TH1572									
MI No.	1	2	3	4	5	6	1	2	3	4	5	6	7	8	9	10
State	UH	H	UH	UH	H	UH	H	H	UH	UH	H	H	H	H	UH	UH
SiO_2	53.4	62.5	37.1	41.0	66.6	35.1	63.2	64.4	35.0	39.6	65.7	68.3	67.8	66.5	39.0	43.2
TiO_2	0.43	0.26	3.17	1.77	0.00	0.64	0.15	0.18	3.08	2.83	0.03	0.00	0.08	0.18	1.44	0.97
Al_2O_3	15.1	18.2	12.6	14.5	17.8	12.5	17.8	17.2	10.2	11.6	17.5	17.3	17.8	18.4	15.2	15.6
FeO_t	8.10	1.88	13.6	10.1	1.13	17.5	1.03	1.58	18.2	13.6	0.80	0.92	0.97	1.17	10.8	8.10
MnO	0.17	0.08	0.10	0.23	0.00	0.33	0.01	0.06	0.23	0.18	0.04	0.03	0.07	0.03	0.18	0.24
MgO	4.35	1.39	5.71	5.31	0.46	4.07	0.38	0.98	6.04	5.93	0.21	0.50	0.47	0.39	6.19	4.58
CaO	7.27	4.54	13.5	11.9	3.28	16.2	7.77	5.94	15.2	14.1	5.55	2.67	3.30	3.60	15.2	15.1
Na_2O	4.95	6.47	4.48	4.88	6.57	2.20	4.74	7.02	3.71	4.26	5.00	7.27	6.84	6.21	2.71	3.45
K_2O	1.32	3.96	1.47	2.43	3.96	2.97	3.05	3.19	0.33	1.24	3.01	4.19	3.44	2.81	3.69	2.74
P_2O_5	2.87	0.30	5.81	4.38	0.35	4.74	2.71	0.43	5.90	5.51	1.42	0.15	0.60	0.41	3.61	4.35
Total	98.00	99.6	97.5	96.5	100	96.2	101	101	97.8	98.8	99.2	101	101	99.7	98.0	98.4

Sample	TH1573							TH1586				TH1589				
MI No.	1	2	3	4	5	6	7	1	2	3	4	1	2	3	4	5
State	UH	UH	UH	H	H	UH	H	H	UH	H	H	H	H	H	UH	UH
SiO_2	43.8	53.8	33.6	63.1	64.7	46.5	61.7	61.4	36.9	56.2	63.0	56.9	62.4	56.8	38.0	32.3
TiO_2	7.19	5.84	1.79	0.05	0.03	4.20	0.09	0.03	4.24	0.01	0.13	0.98	0.28	0.28	2.93	2.89
Al_2O_3	10.2	13.4	12.1	16.1	13.2	11.7	14.4	17.0	10.3	14.7	17.6	17.5	19.00	16.9	12.9	9.10
FeO_t	13.2	7.85	13.9	1.24	1.33	9.75	3.33	2.55	15.4	5.91	1.84	4.25	1.56	2.73	11.2	21.4
MnO	0.21	0.09	0.28	0.04	0.04	0.24	0.12	0.09	0.19	0.09	0.05	0.10	0.05	0.06	0.20	0.25
MgO	2.79	0.78	5.81	0.70	0.82	4.20	2.12	2.15	5.29	2.71	1.22	2.50	1.15	3.57	6.53	5.06
CaO	13.2	8.51	19.2	6.76	7.67	10.9	7.23	6.89	13.0	10.0	6.87	7.60	4.84	6.96	14.0	18.00
Na_2O	3.78	3.77	2.62	4.49	3.86	3.93	3.78	3.53	4.97	3.25	6.19	5.80	7.09	7.01	4.03	2.54
K_2O	0.26	1.90	2.20	4.04	3.87	1.49	3.69	3.56	0.24	3.07	2.63	2.18	3.78	2.66	2.04	0.27
P_2O_5	3.87	1.59	6.74	1.21	2.54	3.90	1.53	1.45	6.22	1.81	1.22	1.97	0.91	2.48	5.68	6.23
Total	98.6	97.5	98.3	97.7	98.0	96.9	98.1	98.6	96.7	97.9	101	99.7	101	99.4	97.5	98.0

Note: MI, melt inclusion; H, homogenized inclusion; UH, unhomogenized inclusion.

intrusion and the nearby peralkaline A-type granite unit are comagmatic and cogenetic and originated through fractional crystallization of a common parental magma resembling the high-Ti Emeishan flood basalts (Shellnutt et al., 2009, 2010, 2011). Mass balance makes the probability of this occurring very low because the volume of the granitic pluton is at least four times larger than that of the mafic layered intrusion (Zhong et al., 2009), i.e., far beyond the usual 5%–10% felsic melts that can be differentiated from basaltic magmas (Veksler, 2009; VanTongeren et al., 2010; Namur et al., 2011). Alternatively, the loss of the Si-rich components could be considered in terms of faulting, folding, denudation, and intrusion (cf., Ashwal et al., 2005). The faults in the Taihe area are NE-SW, NW-SE, and N-S oriented and locally cut through the layering. There are no layer-parallel faults, which would be necessary in order for the faults to explain the loss of Si-rich components. The folding of layered rocks cannot account for the absence of Silica-rich layers in a vertical stratigraphic sequence, as discussed by Wilson et al. (1994). The non-depositional environment of a region could have caused weathering and denudation of the existing geologic body. However, because the fact that the Taihe layered intrusion is totally enclosed from both top to bottom by the homochronous peralkaline A-type granitic pluton makes this explanation impossible. We suggest that the most likely explanation is a magmatic transgression of peralkaline granitic magmas over the layered cumulates. In this model, the uppermost residual magmas were expelled by the emplacement of the peralkaline granitic magmas. The missing Si-rich components may have been physically displaced upwards or, more likely, were entrained into the intruding magmas.

Fine-grained enclaves are common in some areas of the Taihe peralkaline A-type granitic pluton. This is rarely seen in peralkaline A-type granites in general, although enclaves are ubiquitous within peraluminous and metaluminous granites with S- and I-type affinities (Barbarin, 1999). The reason for this difference is unclear, but it may be due to their origins, i.e., enclaves are more likely to form in magma systems with contributions from multiple sources (Shellnutt et al., 2010). S- and I-type granitic rocks are typically derived from crust/mantle interactions involving magma mingling, mixing, and partial

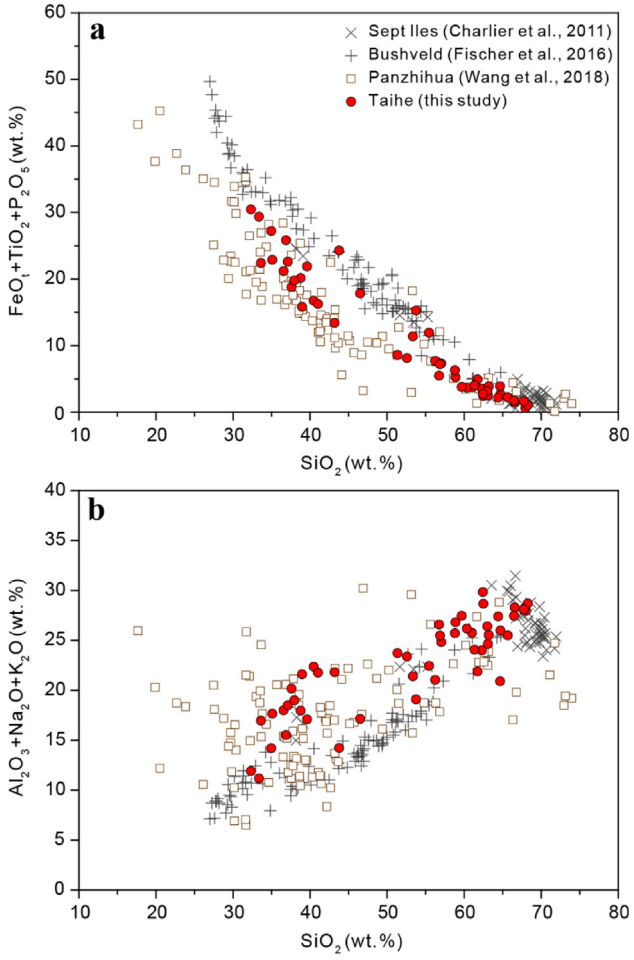

Fig. 7. Plots of FeO_t + TiO_2 + P_2O_5 (a) and Al_2O_3 + Na_2O + K_2O (b) vs. SiO_2 for the apatite-hosted melt inclusions from the Taihe gabbroic layered intrusion. The apatite-hosted melt inclusions from the Panzhihua (Wang et al., 2018), Sept Iles (Charlier et al., 2011), and Bushveld (Fischer et al., 2016) intrusions are shown for comparison.

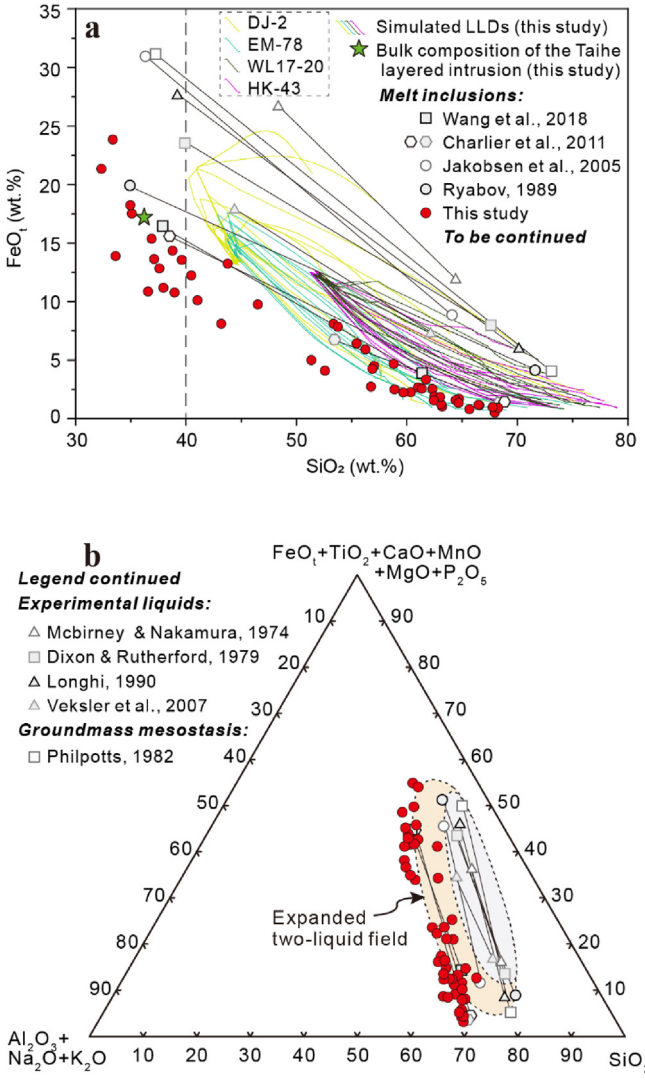

Fig. 8. Compositional variation of the apatite-hosted melt inclusions from the Taihe gabbroic layered intrusion. Tie lines of the conjugate immiscible melt pairs from melt inclusions, experiments and groundmass mesostasis are shown for comparison. (a) Plot of FeO_t vs. SiO_2 showing potential liquid line of descent (LLD) for the Taihe layered intrusion. Four-group different colors of lines represent the differentiated melt compositions of MELTS calculations (Ghiorso and Sack, 1995) for four different starting compositions of DJ-2, EM-78, WL17-20, and HK-43 (see Table 2) with initial H_2O contents of 0.1 wt% and 1.0 wt% at oxygen fugacity conditions of QFM-1, QFM, and QFM + 1, and pressures of 2 kbar and 5kbar. A green five-pointed star represents the calculated bulk composition (BC) of the Taihe gabbroic intrusion. (b) Pseudo-ternary diagram [(FeO_t + TiO_2 + CaO + MnO + MgO + P_2O_5) -(Al_2O_3 + Na_2O + K_2O) -P_2O_5] with an extended two-liquid field. The gray area is the two-liquid field (gray area) in the system of leucite-fayalite-silica (Roedder, 1951). The peahpuff colored area indicates the enlarged part of two-liquid field in the natural basaltic magma system, which is confined by the apatite-hosted immiscible melts inclusions from the Sept Iles and Panzhihua intrusions (Charlier et al., 2011; Wang et al., 2018). (For interpretation of the references to colour in this figure legend, the reader is referred to the web version of this article.)

melting of the crust with heterogeneous compositions, whereas most peralkaline A-type granitic rocks are formed by simple fractional crystallization of a single mantle-derived magma.

The enclaves within the Taihe peralkaline A-type granites were previously considered to be accumulations of minerals formed earlier (compared with the granites) during the differentiation of the gabbroic rocks into the granites within the Taihe gabbro-granite complex (Shellnutt et al., 2010). Although the decrease in the Mg content (apfu) of the amphibole from the gabbros to the enclaves and peralkaline granites (Fig. 9a) may be reconciled with fractional crystallization, the obvious compositional gap in the plot of Ca/(Ca + Na + K) vs. Si (apfu) (Fig. 9b) cannot be accounted for by a continuous fractional crystallization process. It suggests a sudden change in the physical–-chemical conditions of the related magmas. Sodic-calcic and sodic amphiboles are stable only in very late magmatic stages and even during hydrothermal activity when the system is very rich in volatiles at relatively low temperatures (Charles, 1975, 1977; Ferguson, 1978; Giret et al., 1980). If the uppermost Si-rich residual magmas that differentiated from the Taihe layered intrusion were entrained by the intruding peralkaline A-type granitic magmas, the typical products of this interaction would be the igneous enclaves. The ellipsoidal shapes and fine-grained texture of the silicic enclaves within the Taihe granitic pluton indicate that they were plastic and experienced rapid cooling. In this scenario, considerable equilibration could have occurred between the lost Si-rich melts and the peralkaline A-type granitic magmas (high F contents of 1.1 ± 0.1 wt%; Shellnutt and Iizuka, 2011), and the most prominent effect on the enclave melts might be the increase in volatiles and the decrease in temperature, which would cause the crystallization of sodic-calcic amphiboles (Fig. 9b). Thus, we consider the enclaves within the adjacent A-type peralkaline granites to be the missing Si-rich melts from the Taihe layered intrusion.

Table 2
Bulk composition (wt.%) of the Taihe layered intrusion and other high-Fe mafic magmas.

	Taihe[1]	Taihe[2]	High-Ti picrite[3]	High-Ti basalt[4]	High-Ti basalt[5]	High-Ti basalt[6]	Bushveld[7]	Skaergaard[8]	Sept Iles[9]	East Greenland lava[10]	Pechenga [11]
SiO_2	36.20	43.10	44.47	44.37	50.55	49.62	49.79	48.82	48.53	47.90	46.50
TiO_2	4.78	4.10	2.35	3.15	4.58	3.89	0.82	2.24	2.82	4.40	2.29
Al_2O_3	13.47	15.50	11.15	14.95	12.28	12.86	15.82	14.42	14.67	12.50	10.10
FeO^t	17.24	14.13	11.09	13.91	12.07	12.10	11.71	12.13	14.50	14.31	14.04
MnO	0.19			0.20	0.18	0.13		0.18	0.21		
MgO	7.10	5.40	14.78	7.27	4.48	3.48	6.14	6.06	5.65	5.49	14.80
CaO	13.53	12.20	11.38	10.78	6.77	5.89	10.93	12.57	9.79	10.00	8.62
Na_2O	1.62	2.60	1.89	2.26	3.63	4.54	2.97	3.01	2.63	2.72	0.40
K_2O	0.44	0.50	0.08	1.23	1.74	2.45	0.25	0.38	0.77	0.64	1.03
P_2O_5	1.09	0.50	0.34	0.34	0.47	0.59	0.07	0.20	0.82	0.45	0.21
Mg#	42.57	40.76	70.58	48.47	40.05	34.11	48.56	47.35	41.22	40.85	65.49

Notes:
1. Bulk composition of the Taihe intrusion including ore bodie (this study).
2. Bulk composition of the Taihe intrusion excluding ore bodies (Hou et al., 2012).
3. Emeishan high-Ti picrite(sample DJ-2), Lijiang area(Zhang et al., 2006).
4. Emeishan high-Ti basalt (sample EM-78), Ertan area (Xu et al., 2001).
5. Emeishan high-Ti basalt (sample WL17-20), Binchuan area (Xiao et al., 2004).
6. Emeishan high-Ti basalt (sample HK-43), Songda area (Wang et al., 2007).
7. Parental magma of the Upper Zone and Upper Main Zone of the Bushveld complex (Davies and Cawthorn, 1984).
8. Parental magma of the Skaergaard intrusion (Jakobsen et al., 2010).
9. Parental magma of the Sept Iles intrusion (Namur et al., 2010).
10. Tertiary ferrotholeiite from East Greenland (Larsen et al., 1989).
11. Average of ferropicrites in Pechenga, Finland (Hanski, 1992) Mg# = [molar 100 × Mg/(Mg + Fe)].

6.4. Magma chamber processes resulting in the loss of Si-rich components

In most instances, the cumulate rocks that define a layered intrusion solidify from an initial crystal mush composed of primocrysts and interstitial liquid (e.g., Marsh, 2006; Humphreys, 2011; Holness et al., 2013). The Primocrysts form at the interface between the crystal mush and the crystal-free main magma body. Then, they are entrained into the crystal mush (Namur and Humphreys, 2018). Although the thickness of the crystal mush and its solidification timescale are controversial (McKenzie, 2011; Holness et al., 2017), the initial porosity of the mush is generally considered to be 0.5–0.7 (Irvine, 1980; Philpotts et al., 1998; Jerram et al., 2003).

As was discussed above, the large compositional range of the apatite-hosted melt inclusions indicates that liquid immiscibility occurred during the differentiation of the Taihe layered intrusion. Nevertheless, liquid immiscibility may not have affected the entire mass of liquid at the same time, which would have resulted in simple physical segregation of the emulsified magma chamber into an Fe-rich layer in the lower part of the chamber and a Si-rich layer in the upper part (c.f. VanTongeren and Mathez, 2012). If this is the case, the segregated immiscible Si-rich melts at the top are the most probable candidates for the missing Si-rich components that were removed. However, the silicic enclaves have higher contents of FeO + TiO_2 and similar contents of Na_2O + K_2O to the immiscible Si-rich melt inclusions in the apatite (Fig. 10a and b). This cannot be explained by simple mixing with granitic magma because simple mixing would produce linear trends in all of the major elements. We suggest that immiscibility occurred repetitively in the lower crystal mush with the progressively advancing crystallization fronts within the Taihe mafic magma chamber, as has been suggested for the Sept Iles intrusion (Charlier et al., 2011), the western limb of the Bushveld complex (Fischer et al., 2016), and the Skaergaard intrusion (Namur and Humphreys, 2018).

Immiscible melts composed of high-density Fe-rich melt (2.9–3.1 g/cm^3) with lower-density Si-rich droplets (2.4–2.5 g/cm^3) developed within the crystal mush (Fig. 11a; Namur et al., 2015; Wang et al., 2018). The Si-rich droplets were driven upwards due to compaction and the density difference between the two conjugate melts. The segregation of the conjugate immiscible melts drastically affected the

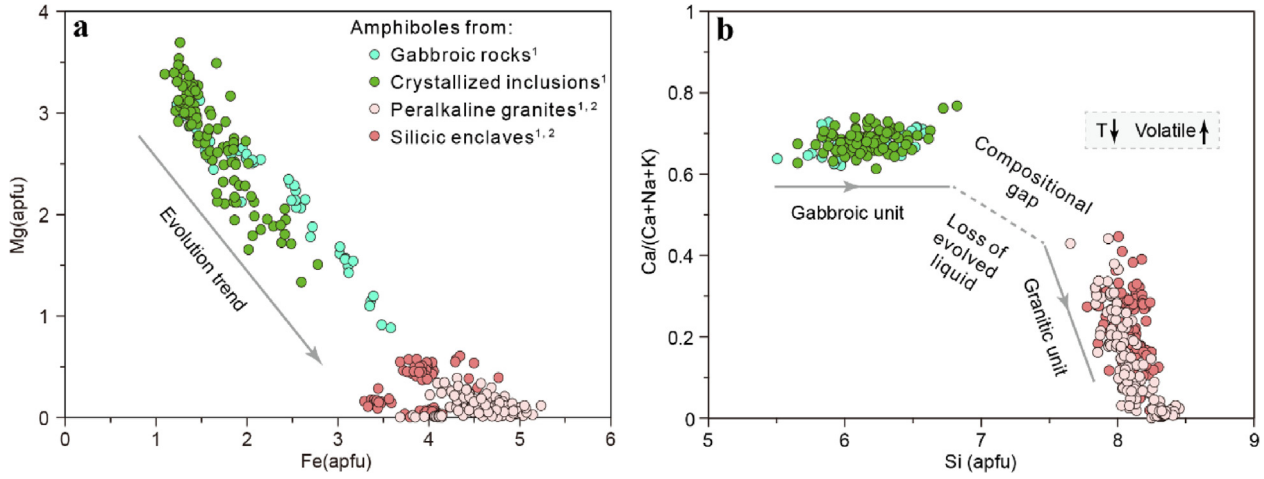

Fig. 9. Compositional variation of the amphiboles from the apatite-hosted crystallized melt inclusions, gabbroic rocks, peralkaline A-type granites, and silicic enclaves. (a) Plot of Mg vs. Fe (apfu = atoms per formula unit); (b) Plot of Ca/(Ca + Na + K) vs. Si (apfu). Data sources: 1. this study; 2. Shellnutt and Iizuka, 2011.

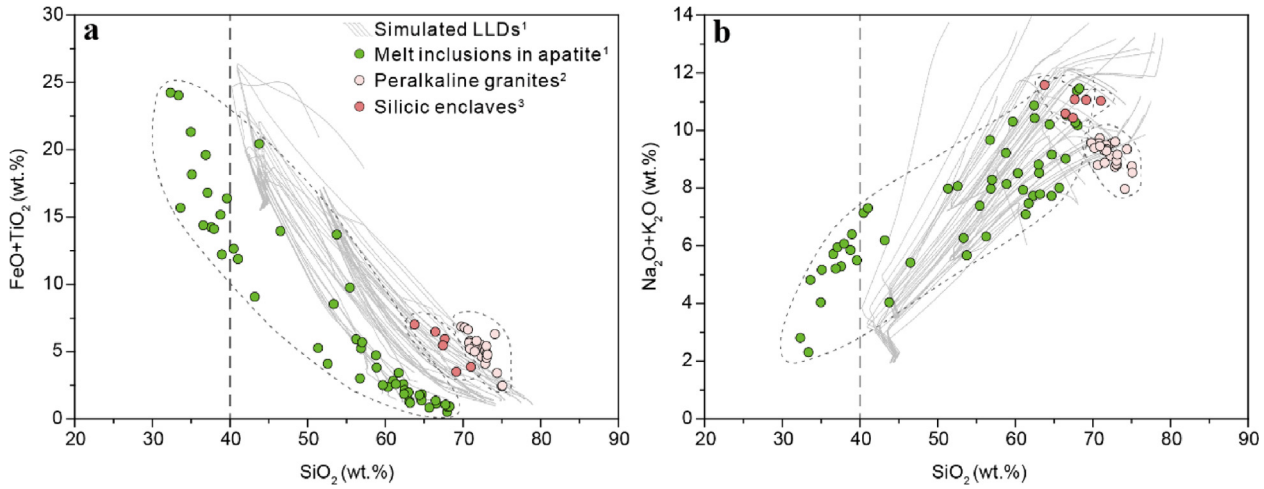

Fig. 10. Plots of FeO + TiO_2 (a) and Na_2O + K_2O (b) vs. SiO_2 for the apatite-hosted melt inclusions, peralkaline A-type granite, and silicic enclaves from the Taihe gabbroic-granitic complex. Gray lines represent the potential liquid line of descent (LLDs) through fractional crystallization of four different starting compositions of DJ-2, EM-78, WL17-20, and HK-43 (see Table 2) with initial H_2O contents of 0.1 wt% and 1.0 wt% at oxygen fugacity conditions of QFM-1, QFM, and QFM + 1, and pressures of 2 kbar and 5kbar. Data sources: 1. this study; 2. Shellnutt et al., 2010; 3. Shellnutt and Zhou, 2007.

solidification of the crystal mush, resulting in the crystallization of large amounts of Fe-Ti oxides from the interstitial Fe-rich liquid, which formed a thick, closely packed layer of Fe-Ti oxides (Fig. 11b; c.f. Humphreys, 2011; Wang et al., 2013, 2018, 2019; Holness et al., 2017; Namur and Humphreys, 2018). The main magma body evolved continually as the primocrysts crystallized at the interface between the magma body and the crystal mush and with the addition of the expelled immiscible Si-rich melts from the lower crystal mush. Neither simple fractional crystallization nor liquid immiscibility, but rather a combined effect, produced the upper residual melt of the magma chamber. Subsequently, peralkaline A-type granitic magma began to intrude into the space adjacent to the Taihe layered intrusion. The residual evolved melts were stirred and entrained into the granitic magma, and equilibration occurred between the enclaves and the host magma (Fig. 11b).

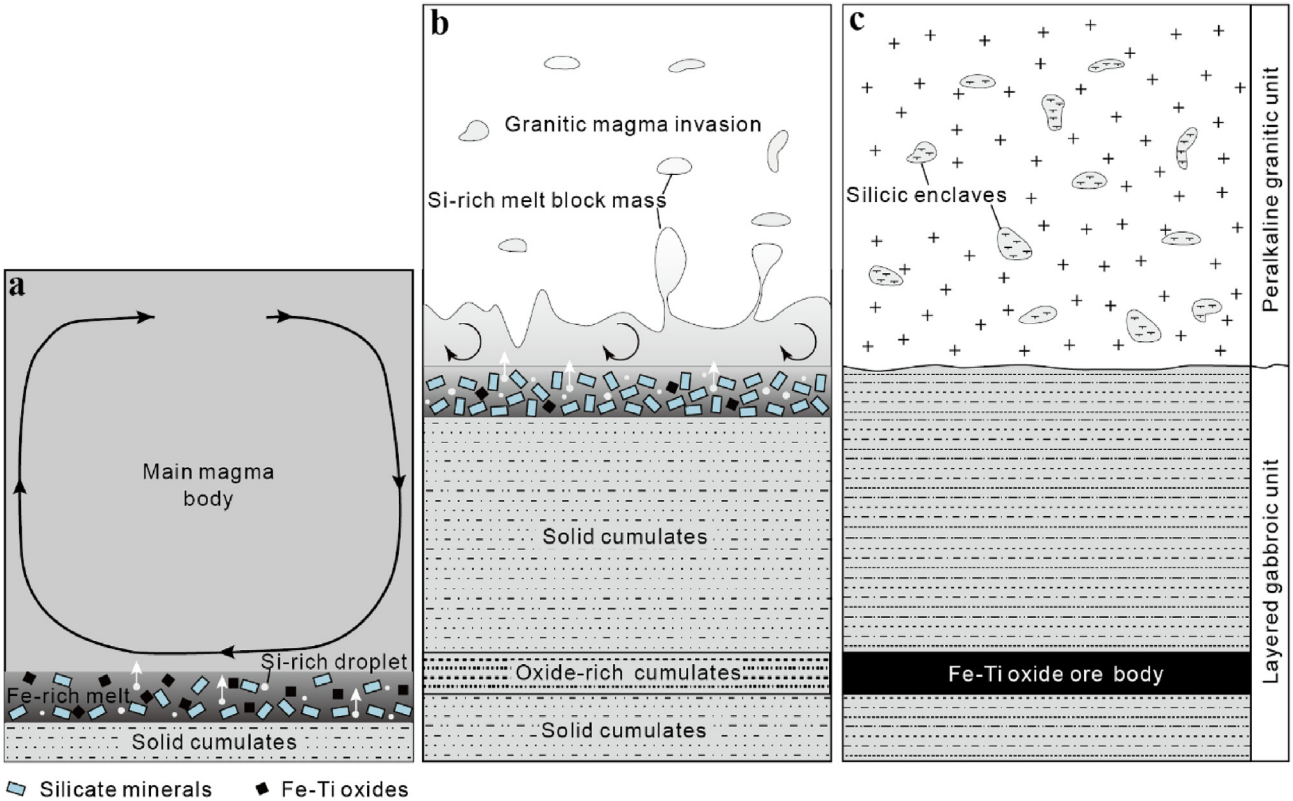

Fig. 11. A cartoon showing the model of magma evolution and the loss of Si-rich components of the Taihe mafic magma chamber. (a) Interstitial liquid within crystal mush intersected two-liquid field and split into emulsified magma with Si-rich droplets and Fe-rich melt after a period of bottom crystallization. (b) Evolved residual Si-rich melts were generated at the top of the magma chamber through the sustained crystallization of the primocrysts and the addition of the immiscible Si-rich melts expelled from the lower crystal mush; and then, they were stirred and captured by the subsequently intruding peralkaline A-type granitic magma. (c) Further crystallization and solidification formed the Taihe layered intrusion with its thick Fe-Ti oxide ore layers and the adjacent peralkaline A-type granitic pluton with its silicic enclaves.

Finally, the mafic and granitic magma units solidified completely and formed the Taihe layered intrusion with its thick Fe-Ti oxide layers and the adjacent Taihe peralkaline A-type granitic pluton with its silicic enclaves (Fig. 11c).

7. Conclusions

The apatite-hosted melt inclusions from the Taihe layered intrusion have a large compositional range, which is attributed to the development of silicate liquid immiscibility within the crystal mush. The main magma body evolved through further crystallization and mixing of immiscible Si-rich melt expelled from the lower crystal mush. The residual evolved melts in the upper part of the magma chamber above the cumulates were entrained by the subsequent intrusion of granitic magma and formed the silicic enclaves in the Taihe granitic pluton. Liquid immiscibility and the loss of a Si-rich component promoted the concentration of Fe, Ti, and P, and thereby contributed to the formation of the Taihe large Fe-Ti oxide deposit.

Declaration of Competing Interest

The authors declare that they have no known competing financial interests or personal relationships that could have appeared to influence the work reported in this paper.

Acknowledgments

This study was financially supported by the Strategic Priority Research Program (B) of the Chinese Academy of Sciences (XDB18000000), the National Natural Science Foundation of China grant (41902082), the China Postdoctoral Science Foundation grant (2019 M652733), and the research grant of State Key Laboratory of Isotope Geochemistry, Guangzhou Institute of Geochemistry, Chinese Academy of Sciences (SKLabIG-KF-18-01). We are sincerely grateful to Prof. Christina Yan Wang for her help in many aspects.We thank Drs. Changming Xing, Yonghua Cao, and Bo Wei for their assistances during the field work. Constructive comments from two anonymous reviewers and careful editorial handling by Franco Pirajno were highly appreciated.

Appendix A. Supplementary data

Supplementary data to this article can be found online at https://doi.org/10.1016/j.oregeorev.2020.103418.

References

Armstrong, R., 1991. The persistent myth of crustal growth. Aust. J. Earth Sci. 38, 613–630.
Ashwal, L.D., Webb, S.J., Knoper, M.W., 2005. Magmatic stratigraphy in the Bushveld Northern Lobe: continuous geophysical and mineralogical data from the 2950 m Bellevue drill core. S. Afr. J. Geol. 108 (2), 199–232.
Bai, Z.J., Zhong, H., Li, C., Zhu, W.G., Hu, W.J., 2016. Association of cumulus apatite with compositionally unusual olivine and plagioclase in the Taihe Fe-Ti oxide ore-bearing layered mafic-ultramafic intrusion: Petrogenetic significance and implications for ore genesis. Am. Mineral. 101, 2168–2175.
Barbarin, B., 1999. A review of the relationship between granitoid types, their origins and their geodynamic environments. Lithos 46, 605–626.
Bonin, B., 2007. A-type granites and related rocks: evolution of a concept, problems and prospects. Lithos 97, 1–29.
Bottinga, Y., Weill, D.F., 1970. Densities of liquid silicate systems calculated from partial molar volumes of oxide components. Am. J. Sci. 269 (2), 169–182.
Carmichael, I.S.E., 1964. The petrology of Thingmuli, a Tertiary volcano in eastern Iceland. J. Petrol. 5, 435–460.
Charles, R.W., 1975. The phase equilibria of richterite and ferrorichterite. Am. Mineral. 60, 367–374.
Charles, R.W., 1977. The phase equilibria of intermediate compositions on the pseudo-binary $Na_2CaMg_5Si_8O_{22}(OH)_2$-$Na_2CaFe_5Si_8O_{22}(OH)_2$. Am. J. Sci. 277 (5), 594–625.
Charlier, B., Namur, O., Toplis, M.J., Schiano, P., Cluzel, N., Higgins, M.D., Auwera, J.V., 2011. Large-scale silicate liquid immiscibility during differentiation of tholeiitic basalt to granite and the origin of the Daly gap. Geology 39, 907–910.
Chung, S.L., Jahn, B.M., 1995. Plume-lithosphere interaction in generation of the Emeishan flood basalts at the Permian-Triassic boundary. Geology 23, 889–892.
Danyushevsky, L.V., McNeill, A.W., Sobolev, A.V., 2002. Experimental and petrological studies of melt inclusions in phenocrysts from mantle-derived magmas: an overview of techniques, advantages and complications. Chem. Geol. 183, 5–24.
Davies, G., Cawtnorn, R.G., 1984. Mineralogical data on a multiple intrusion in the Rustenburg Layered Suite of the Bushveld Complex. Mineral. Mag. 48 (349), 469–480.
Dixon, S., Rutherford, M.J., 1979. Plagiogranites as late-stage immiscible liquids in ophiolite and mid-ocean ridge suites: An experimental study. Earth Planet. Sci. Lett. 45, 45–60.
Eby, G.N., 1980. Minor and trace element partitioning between immiscible ocelli-matrix pairs from lamprophyre dikes and sills, Monteregian Hills petrographic province. Quebec. Contrib. Mineral. Petrol. 75, 269–278.
Esawi, E.K., 2004. AMPH-CLASS: An Excel spreadsheet for the classification and nomenclature of amphiboles based on the 1997 recommendations of the International Mineralogical Association. Comput. Geosci. 30 (7), 753–760.
Ferguson, A.K., 1978. The crystallization of pyroxenes and amphiboles in some alkaline rocks and the presence of a pyroxene compositional gap. Contrib. Mineral. Petrol. 67 (1), 11–15.
Fischer, L.A., Wang, M., Charlier, B., Namur, O., Roberts, R.J., Veksler, I.V., Cawthorn, R.G., Holtz, F., 2016. Immiscible iron- and silica-rich liquids in the Upper Zone of the Bushveld Complex. Earth Planet. Sci. Lett. 443, 108–117.
Freestone, I.C., 1978. Liquid immiscibility in alkali-rich magmas Chem. Geol. 23, 115–123.
Ghiorso, M.S., Sack, R.O., 1995. Chemical mass transfer in magmatic processes IV. A revised and internally consistent thermodynamic model for the interpolation and extrapolation of liquid-solid equilibria in magmatic systems at elevated temperatures and pressures. Contrib. Mineral. Petrol. 119 (2–3), 197–212.
Giret, A., Bonin, B., Leger, J.M., 1980. Amphibole compositional trends in oversaturated and undersaturated alkaline plutonic ring-composition. Can. Mineral. 18 (4), 481–495.
Hanski, E.J., 1992. Petrology of the Pechenga ferropicrites and cogenetic, Ni-bearing gabbro-wehrlite intrusions, Kola Peninsula. Russia. Bull. Geol. Surv. Finland 367, 192.
Holness, M.B., Cawthorn, R.G., Roberts, J., 2017. The thickness of the crystal mush on the floor of the Bushveld magma chamber. Contrib. Mineral. Petrol. 172, 102.
Holness, M.B., Namur, O., Cawthorn, R.G., 2013. Disequilibrium dihedral angles in layered intrusions: a microstructural record of fractionation. J. Petrol. 54, 2067–2093.
Hou, T., Zhang, Z., Encarnacion, J., Santosh, M., 2012. Petrogenesis and metallogenesis of the Taihe gabbroic intrusion associated with Fe–Ti-oxide ores in the Panxi district, Emeishan Large Igneous Province, southwest China. Ore Geol. Rev. 49, 109–127.
Hou, T., Zhang, Z., Ye, X., Encarnacion, J., Reichow, M.K., 2011. Noble gas isotopic systematics of Fe–Ti–V oxide ore-related mafic–ultramafic layered intrusions in the Panxi area, China: The role of recycled oceanic crust in their petrogenesis. Geochim. Cosmochim. Acta 75, 6727–6741.
Humphreys, M.C.S., 2011. Silicate liquid immiscibility within the crystal mush: evidence from Ti in plagioclase from the Skaergaard intrusion. J. Petrol. 52, 147–174.
Irvine, T.N., 1980. Magmatic infiltration metasomatism, double-diffusive fractional crystallization, and adcumulus growth in the Muskox intrusion and other layered Intrusions. In: Hargraves, R.B. (Ed.), Physics of Magmatic Processes. Princeton University Press, Princeton, NJ, pp. 325–384.
Jakobsen, J.K., Tegner, C., Brooks, C.K., Kent, A.J., Lesher, C.E., Nielsen, T.F., Wiedenbeck, M., 2010. Parental magma of the Skaergaard intrusion: constraints from melt inclusions in primitive troctolite blocks and FG-1 dykes. Contrib. Mineral. Petrol. 159 (1), 61.
Jakobsen, J.K., Veksler, I.V., Tegner, C., Brooks, C.K., 2011. Crystallization of the Skaergaard intrusion from an emulsion of immiscible iron-and silica-rich liquids: evidence from melt inclusions in plagioclase. J. Petrol. 52, 345–373.
Jerram, D.A., Cheadle, M.J., Philpotts, A.R., 2003. Quantifying the building blocks of igneous rocks: are clustered crystal frameworks the foundation? J. Petrol. 44, 2033–2051.
Kent, A.J., 2008. Melt inclusions in basaltic and related volcanic rocks. Rev. Mineral. Geochem. 69 (1), 273–331.
Kushiro, I., 1979. Fractional crystallization of basaltic magma. In: Yoder, H.S. (Ed.), The Evolution of the Igneous Rocks. Princeton University Press, Princeton, NJ, pp. 171–203.
Larsen, L.M., Watt, W.S., Watt, M., 1989. Geology and Petrology of the Lower Tertiary Plateau Basalts of the Scoresby Sund Region. East Greenland. Bull. Grønl. Geol. Unders. 157, 164.
Leake, B.E., Woolley, A.R., Birch, W.D., Burke, E.A., Ferraris, G., Grice, J.D., Hawthorne, F.C., Kisch, H.J., Krivovichev, V.G., Schumacher, J.C., Stephenson, N.C., Whittaker, Eric J.W., 2004. Nomenclature of amphiboles: additions and revisions to the International Mineralogical Association's amphibole nomenclature. Am. Mineral. 89, 883–887.
Li, D.H., Chen, Z.X., Han, Z.W., 1981. The cyclothem and petrographic characteristics of the Taihe layered intrusion in Xichang. J. Chengdu Univ. Technol. (Nature Science Edition) 3, 9–21 (in Chinese).
Liu, P.P., Zhou, M.F., Ren, Z.Y., Wang, C.Y., Wang, K., 2016. Immiscible Fe- and Si-rich silicate melts in plagioclase from the Baima mafic intrusion (SW China): Implications for the origin of bi-modal igneous suites in large igneous provinces. J. Asian Earth Sci. 127, 211–230.
Longhi, J., 1990. Silicate liquid immiscibility in isothermal crystallization experiments. Lunar and Planetary Sci. Conf. Proc. 13–24.
Ma, Y.X., Ji, X.T., Li, J.C., Huang, M., Min, Z.Z., 2003. Mineral resources of Panzhihua,

Sichuan Province, SW China. Chengdu University of Technology Press, Chengdu, pp. 1–275 (in Chinese).
Marsh, B.D., 2006. Dynamics of magmatic systems. Elements 2, 287–292.
McKenzie, D., 2011. Compaction and crystallization in magma chambers: towards a model of the Skaergaard intrusion. J. Petrol. 52, 905–930.
McBirney, A.R., Nakamura, Y., 1974. Immiscibility in late-stage magmas of the Skaergaard intrusion. Carnegie Institution of Washington Yearbook 73, 348–352.
Namur, O., Abily, B., Boudreau, A., Blanchette, F., Bush, J.W.M., Ceuleneer, G., Charlier, B., Donaldson, C.H., Duchesne, J.C., Higgins, M.D., Morata, D., Nielsen, T.F.D., O'Driscoll, B., Pang, K.N., Peacock, T., Spandler, C., Toramaru, A., Veksler, I.V., 2015. Igneous layering in basaltic magma chambers. In: Charlier, B. (Ed.), Layered intrusions. Springer, Dordrecht, pp. 75–152.
Namur, O., Charlier, B., Toplis, M.J., Higgins, M.D., Liégeois, J.P., Vander Auwera, J., 2010. Crystallization sequence and magma chamber processes in the ferrobasaltic Sept Iles layered intrusion. Canada. J. Petrol. 51 (6), 1203–1236.
Namur, O., Charlier, B., Toplis, M.J., Higgins, M.D., Hounsell, V., Liégeois, J.P., Vander Auwera, J., 2011. Differentiation of tholeiitic basalt to A-type granite in the Sept Iles layered intrusion. Canada. J. Petrol. 52 (3), 487–539.
Namur, O., Humphreys, M.C., 2018. Trace element constraints on the differentiation and crystal mush solidification in the Skaergaard intrusion. Greenland. J. Petrol. 59 (3), 387–418.
Naslund, H.R., 1983. The Effect of Oxygen Fugacity on Liquid Immiscibility in Iron-Bearing Silicate Melts. Am. J. Sci. 283, 1034–1059.
Pang, K.N., Li, C., Zhou, M.F., Ripley, E.M., 2009. Mineral compositional constraints on petrogenesis and oxide ore genesis of the late Permian Panzhihua layered gabbroic intrusion. SW China. Lithos 110 (1–4), 199–214.
Philpotts, A.R., 1982. Compositions of immiscible liquids in volcanic rocks. Contrib. Mineral. Petrol. 80, 201–218.
Philpotts, A.R., Shi, J., Brustman, C., 1998. Role of plagioclase crystal chains in the differentiation of partly crystallized basaltic magma. Nature 395 (6700), 343–346.
Qiu, R.X., Xie, S.M., 1988. Application of the ratios of TFe/TiO_2 to the exploration of the Panzhihua Fe-Ti-V oxide deposit. Acta Geol. Sichuan 18, 53–59 (in Chinese).
Rajesh, H.M., 2003. Outcrop-scale silicate liquid immiscibility from an alkali syenite (A-type granitoid)-pyroxenite association near Puttetti, Trivandrum Block, South India. Contrib. Mineral. Petrol. 145, 612–627.
Ren, Z.Y., Wu, Y.D., Zhang, L., Nichols, A.R.L., Hong, L.B., Zhang, Y.H., Zhang, Y., Liu, J.Q., Xu, Y.G., 2017. Primary magmas and mantle sources of Emeishan basalts constrained from major element, trace element and Pb isotope compositions of olivine-hosted melt inclusions. Geochim. Cosmochim. Acta 208, 63–85.
Roedder, E., 1951. low temperature liquid immiscibility in the system K_2O-FeO-Al_2O_3-SiO_2. Am. Mineral. 36, 282–286.
Ryabov, V.V., 1989. Liquation in Natural Glasses: The Example of Traps. Nauka, Novosibirsk (in Russian).
She, Y.W., Song, X.Y., Yu, S.Y., He, H.L., 2015. Variations of trace element concentration of magnetite and ilmenite from the Taihe layered intrusion, Emeishan large igneous province, SW China: Implications for magmatic fractionation and origin of Fe-Ti-V oxide ore deposits. J. Asian Earth Sci. 113, 1117–1131.
She, Y.W., Yu, S.Y., Song, X.Y., Chen, L.M., Zheng, W.Q., Luan, Y., 2014. The formation of P-rich Fe–Ti oxide ore layers in the Taihe layered intrusion, SW China: Implications for magma-plumbing system process. Ore Geol. Rev. 57, 539–559.
Shellnutt, J.G., Iizuka, Y., 2011. Mineralogy from three peralkaline granitic plutons of the Late Permian Emeishan large igneous province (SW China): evidence for contrasting magmatic conditions of A-type granitoids. Eur. J. Mineral. 23 (1), 45–61.
Shellnutt, J.G., Jahn, B.M., Dostal, J., 2010. Elemental and Sr-Nd isotope geochemistry of microgranular enclaves from peralkaline A-type granitic plutons of the Emeishan large igneous province, SW China. Lithos 119, 34–46.
Shellnutt, J.G., Wang, K.L., Zellmer, G.F., Iizuka, Y., Jahn, B.M., Pang, K.N., Qi, L., Zhou, M.F., 2011. Three Fe-Ti oxide ore-bearing gabbro-granitoid complexes in the Panxi region of the Permian Emeishan large igneous province. SW China. Am. J. Sci. 311 (9), 773–812.
Shellnutt, J.G., Zhou, M.F., 2007. Permian peralkaline, peraluminous and metaluminous A-type granites in the Panxi district, SW China: Their relationship to the Emeishan mantle plume. Chem. Geol. 243, 286–316.
Shellnutt, J.G., Zhou, M.F., Zellmer, G.F., 2009. The role of Fe–Ti oxide crystallization in the formation of A-type granitoids with implications for the Daly gap: an example from the Permian Baima igneous complex. SW China. Chem. Geol. 259 (3–4), 204–217.
Tegner, C., Cawthorn, R.G., Kruger, F.J., 2006. Cyclicity in the Main and Upper Zones of the Bushveld Complex, South Afica: Crystallization from a zoned magma sheet. J. Petrol. 47, 2257–2279.
VanTongeren, J.A., Mathez, E.A., 2012. Large-scale liquid immiscibility at the top of the Bushveld Complex, South Africa. Geology 40 (6), 491–494.
Vantongeren, J.A., Mathez, E.A., Kelemen, P.B., 2010. A felsic end to Bushveld differentiation. J. Petrol. 51 (9), 1891–1912.
Veksler, I.V., 2009. Extreme iron enrichment and liquid immiscibility in mafic intrusions: experimental evidence revisited. Lithos 111 (1–2), 72–82.
Veksler, I.V., Dorfman, A.M., Borisov, A.A., Wirth, R., Dingwell, D.B., 2007. Liquid Immiscibility and the Evolution of Basaltic Magma. J. Petrol. 48, 2187–2210.
Visser, W., Van Groos, A.K., 1979. Effects of P_2O_5 and TiO_2 on Liquid-Liquid Equilibria in the System K_2O-FeO-Al_2O_3-SiO_2. Am. J. Sci. 279, 970–988.
Wang, K., Dong, H., Liu, R., 2019. Genesis of giant Fe-Ti oxide deposits in the Panxi region. A review. Geol. J, SW China, pp. 1–14.
Wang, K., Wang, C.Y., Ren, Z.Y., 2018. Apatite-hosted melt inclusions from the Panzhihua gabbroic-layered intrusion associated with a giant Fe–Ti oxide deposit in SW China: insights for magma unmixing within a crystal mush. Contrib. Mineral. Petrol. 173 (7), 59.
Wang, K., Xing, C.M., Ren, Z.Y., Wang, Y., 2013. Liquid immiscibility in the Panzhihua mafic layered intrusion: Evidence from melt inclusions in apatite. Acta Petrol. Sin. 29 (10), 3503–3518 (in Chinese with English abstract).
Wang, C.Y., Zhou, M.F., Qi, L., 2007. Permian flood basalts and mafic intrusions in the Jinping (SW China)–Song Da (northern Vietnam) district: mantle sources, crustal contamination and sulfide segregation. Chem. Geol. 3 (243), 317–343.
Wilson, J.R., Cawthorn, R.G., Kruger, F.J., Grundvig, S., 1994. Intrusive origin for the unconformable Upper Zone in the Northern Gap, western Bushveld Complex. S. Afr. J. Geol. 97, 462–472.
Xiao, L., Xu, Y.G., Mei, H.J., Zheng, Y.F., He, B., Pirajno, F., 2004. Distinct mantle sources of low-Ti and high-Ti basalts from the western Emeishan large igneous province, SW China: implications for plume–lithosphere interaction. Earth Planet. Sci. Lett. 228 (3–4), 525–546.
Xu, Y.G., Luo, Z.Y., Huang, X.L., He, B., Xiao, L., Xie, L.W., Shi, Y.R., 2008. Zircon U-Pb and Hf isotope constraints on crustal melting associated with the Emeishan mantle plume. Geochim. Cosmochim. Acta 72, 3084–3104.
Xu, Y.G., Chung, S.L., Jahn, B.M., Wu, G.Y., 2001. Petrologic and geochemical constraints on the petrogenesis of Permian-Triassic Emeishan flood basalts in southwestern China. Lithos 58, 145–168.
Yoder Jr, H., Tilley, C.E., 1962. Origin of basalt magmas: an experimental study of natural and synthetic rock systems. J. Petrol. 3, 342–532.
Zhang, Y.X., Lou, Y., Yang, X., 1988. In: The Panxi Rift. Geological Press, Beijing, pp. 422 (in Chinese).
Zhang, Z., Mahoney, J.J., Mao, J., Wang, F., 2006. Geochemistry of Picritic and Associated Basalt Flows of the Western Emeishan Flood Basalt Province. China. J. Petrol. 47, 1997–2019.
Zhong, H., Campbell, I.H., Zhu, W.G., Allen, C.M., Hu, R.Z., Xie, L.W., He, D.F., 2011. Timing and source constraints on the relationship between mafic and felsic intrusions in the Emeishan large igneous province. Geochim. Cosmochim. Acta 75, 1374–1395.
Zhong, H., Zhu, W.G., Chu, Z.Y., He, D.L., Song, X.Y., 2007. Shrimp U-Pb zircon geochronology, geochemistry, and Nd–Sr isotopic study of contrasting granites in the Emeishan large igneous province, SW China. Chem. Geol. 236, 112–133.
Zhong, H., Xu, G.W., Zhu, W.G., Hu, R.Z., He, D.F., 2009. Petrogenesis of the Taihe Granites in the Emeishan Large Igneous Province and Its tectonic implication. Bull. China Soc. Mineral. Petrol. Geochem. 28, 99–110 (in Chinese).
Zhou, M.F., Chen, W.T., Wang, C.Y., Prevec, S.A., Liu, P., Howarth, G.H., 2013. Two stages of immiscible liquid separation in the formation of Panzhihua-type Fe-Ti-V oxide deposits, SW China. Geosci. Front. 4, 481–502.